Nield, J.M., Wiggs, G.F.S., King, J., Bryant, R.G., Eckardt, F.D., Thomas, D.S.G., Washington, R. (2016) Climate-surface-pore-water interactions on a salt crusted playa: implications for crust pattern and surface roughness development measured using terrestrial laser scanning. Earth Surface Processes and Landforms, 41: 738-753.

Climate-surface-pore-water interactions on a salt crusted playa: implications for crust pattern and surface roughness development measured using terrestrial laser scanning

Joanna M. Nield[1*], Giles F.S. Wiggs[2], James King[2,6], Robert G. Bryant[3], Frank D. Eckardt[4], David S.G. Thomas[2,4,5], Richard Washington[2]

**Corresponding author: Email: J.Nield@soton.ac.uk; Tel: +44 23 8059 4749*

[1] Geography and Environment, University of Southampton, Highfield, Southampton, SO17 1BJ, UK

[2] School of Geography and the Environment, Oxford University Centre for the Environment, University of Oxford, Oxford, OX1 3QY, UK

[3] Department of Geography, University of Sheffield, Sheffield, S10 2TN, UK

[4] Department of Environmental and Geographical Science, University of Cape Town, Rondebosch 7701, South Africa

[5] Geography, Archaeology and Environmental Studies, University of the Witwatersrand, Johannesburg 2050, South Africa

[6] Département de géographie, Université de Montréal, Montréal, QC, H3C 3J7, Canada

Abstract

Sodium accumulating playas (also termed sodic or natric playas) are typically covered by polygonal crusts with different pattern characteristics, but little is known about the short-term (hours) dynamics of these patterns or how pore water may respond to or drive changing salt crust patterning and surface roughness. It is important to understand these interactions because playa-crust surface pore-water and roughness both influence wind erosion and dust emission through controlling erodibility and erosivity. Here we present the first high resolution (10^{-3}m; hours) co-located measurements of changing moisture and salt crust topography using terrestrial laser scanning (TLS) and infra-red imagery for Sua Pan, Botswana. Maximum nocturnal moisture pattern change was found on the crests of ridged surfaces during periods of low temperature and high relative humidity. These peaks experienced non-elastic expansion overnight, of up to 30 mm and up to an average of 1.5 mm/night during the 39 day measurement period. Continuous crusts on the other hand showed little nocturnal change in moisture or elevation. The dynamic nature of salt crusts and the complex feedback patterns identified emphasise how processes both above and below the surface may govern the response of playa surfaces to microclimate diurnal cycles.

Key Words: sodium sulphate, terrestrial laser scanning (TLS), aeolian dust source, playa polygon ridge dynamics, wind erosion

Introduction

Playas (or salt pans; see Briere, 2000) are common in dryland landscapes and typically form salt or clay crusts which exhibit variable moisture both spatially and temporally (Bryant, 2013; Cahill et al., 1996; Gillette et al., 2001; King et al., 2011; Nickling and Ecclestone, 1981; Nickling, 1984). Quantifying moisture within salt containing crusts and sediments on playas is important because it is a major contributor to uncertainty in: i) surface energy and moisture balances (Bryant and Rainey, 2002; Burrough et al., 2009) ii) dust emission (Baddock et al., 2009; Bullard et al., 2011; Haustein et al., 2015; Prospero et al., 2002; Washington et al., 2003; Washington et al., 2006) and iii) salt accumulation rates and styles (Rosen, 1994; Tyler et al., 2006). We know that salt crusts can influence surface topography and patternation on playa surfaces in both a profound and rapid manner (crusts can develop at a rate of as much as 30 mm/week; Nield et al., 2015). Once developed, surface salt crust patterns can significantly alter surface and aerodynamic roughness and ultimately dust emission thresholds (Darmenova et al., 2009; Lancaster, 2004; MacKinnon et al., 2004; Marticorena and Bergametti, 1995; Nield et al., 2013b). Although remote sensing studies have attempted to depict crust moisture and roughness variability on playas over monthly timescales (Archer and Wadge, 2001; Bryant, 1999; Mahowald et al., 2003; Tollerud and Fantle, 2014; Wadge and Archer, 2002; Wadge and Archer, 2003); the results show significant spatial/temporal variability and are far from straightforward to interpret. Ultimately, we know very little about the small-scale temporal (hours) and spatial (mm) dynamics of interstitial or pore moisture patterns on playas, and how the interaction of the moisture with evaporite minerals relates to the development of both crust topography and subsequent crust pattern decay (Groeneveld et al., 2010; Webb and Strong, 2011).

Polygonal salt crusts (Figure 1) are commonly found on playas (Reeves, 1969), including at Owens Lake, USA (Gillette et al., 2001; Saint-Amand et al., 1986; Saint-Amand et al., 1987), Lake Eyre Australia (Bonython, 1956), and in the Atacama desert (Stoertz and Ericksen, 1974). Polygonal pressure ridges form when expansive evaporite minerals precipitate at the surface of a playa through a combination of thermodynamic and geochemical mechanisms (Kendall and Warren, 1987; Krinsley, 1970; Lowenstein and Hardie, 1985; Pakzad and Kulke, 2007; Reeves, 1969). The accumulation of evaporite minerals on a playa surface is broadly controlled by a combination of water table depth, evaporation rates and the salinity/geochemistry of shallow groundwater; which is itself a function of basin inflow/closure (Tyler *et al.*, 1997). Therefore playas with the most erodible crusts (providing opportunity for significant dust flux) typically form when saline groundwater is in close proximity to the playa surface (often < 1m); thereby maximising the impact of evaporation rates on the underlying groundwater, which can lead to movement of salts upwards through the sediment pile, development/breakdown of clay-rich sedimentary fabrics, and ultimately salt deposition at the surface (Buck et al., 2011; Reynolds et al., 2007; Rosen, 1994). In these cases, salt accumulation at the surface of playas can take place over time-scales ranging from hours to many thousands of years through free evaporation at the surface driving the movement and precipitation of evaporite minerals within the shallow capillary fringe (Tyler *et al.,* 1997).

Playa surfaces dominated by sodium-rich salts can be particularly responsive to changes in surface moisture/pore water (Legates et al., 2011; Pelletier, 2006; Reynolds et al., 2007) as these salts (both sodium carbonates and sulphates) readily alter their phase in response to threshold changes in temperature and humidity (Saint-Amand *et al.,* 1986). For example, the dehydrated salt thenardite (Na_2SO_4) can hydrate to form mirabilite ($Na_2SO_4 \bullet 10H_2O$) which typically develops and remains stable when relative humidity exceeds 60 - 75% (the equilibrium or deliquescence relative humidity RH_{eq}) and where temperatures range between 0 and 20°C (Kracek, 1928; Steiger and Asmussen, 2008). Indeed, it is typical for hydrated phases of sodium sulphate and sodium carbonate salts to decrease in solubility as temperature falls (e.g. Benavente et al., 2015). Ultimately, when reduction in temperature is rapid, the phase change to hydrated Na_2-SO_4/Na-$_2CO_3$ phases (e.g. thenardite →mirabilite) can lead to an increase in the size of deposited salt crystals, often by fourfold or more, and is often accompanied by significant changes to the crystallisation pressure (Benavente et al., 2015; Saint-Amand et al., 1986; Tsui et al., 2003) resulting in further changes to internal surface crust structure, surface crust expansion and cracking. Within most playa systems (particularly those with pore water chemistry dominated by Na-CO_3-SO_4-Cl) a range of indicative hydration/dehydration evaporite mineral phase transitions may be achieved both within playa crusts (Drake, 1995; Eugster and Jones, 1979; Eugster and Smith, 1965) and the dust particles that they produce (Jentzsch et al., 2013).

The microclimates of desert playas can be extreme with atmospheric- and pore-moisture fluctuating diurnally in response to changes in relative humidity, temperature, and depth to ground water. High diurnal temperature ranges mean that fluctuations in playa surface pore-water concentration and chemistry are particularly significant both overnight and early in the morning (Groeneveld et al., 2010; Kampf et al., 2005). This general change in moisture availability at the sediment surface can be manifested either within the chemical structure of the evaporite minerals or as free water within the pores of the crust fabric (Mees *et al.,* 2011). On playa surfaces, moisture transfer can occur both above and below any apparent crust through evaporation, capillary transport (Benavente et al., 2004; Benavente et al., 2011; Genkinger and Putnis, 2007; Grossi et al., 2011; Rodriguez-Navarro et al., 2000), and occasionally surface condensation (Kinsman, 1976; Thorburn et al., 1992). The effectiveness of these transfer processes depends on the geochemistry, the internal structure of the crust (e.g. pore connectivity), the shape of the crust (as depicted in Figure 1), and the degree of connectivity between the crust and the underlying moist substrate (Peck, 1960; Turk, 1975). Thus, as a salt crust develops at the surface through precipitation of evaporite minerals, surface roughness and subsurface texture/connectivity can change dramatically. In addition, changes to the relative contribution of moisture inputs from release of water of hydrated minerals, as well as atmospheric or soil/groundwater sources are also apparent (Sanchez-Moral *et al.,* 2002). In particular, continuous, sealed crusts may reduce evaporation from the playa surface to extremely low levels (Gran et al., 2011; Groeneveld et al., 2010; Tyler et al., 1997). Conversely, degraded, cracked or discontinuous crusts may encourage or control the spatial distribution of evaporation, moisture flux and surface efflorescence (Krinsley, 1970).

Terrestrial laser scanning (TLS) is a non-invasive tool (Buckley *et al.*, 2008) that is able to provide high resolution spatial information (millimetres) about salt crust surface change through time, both in terms of topography (Nield *et al.,* 2015) and also various characteristics of surface properties derived from the intensity of the return signal (Lichti, 2005), including surface moisture (Armesto-González et al., 2010; Nield et al., 2011; Nield and Wiggs, 2011). Time-lapse cameras are also useful for examining changes in surface patterns. For example they have been used to identify i) ripple migration (Lorenz, 2011; Lorenz and Valdez, 2011), ii) salt crystal formation in heritage buildings (Zehnder and Schoch, 2009)) and iii) surface moisture (Darke et al., 2009; Darke and Neuman, 2008; McKenna Neuman and Langston, 2006).

Here, for the first time, we seek to untangle the behaviour of playa surfaces; and in particular surface, pore or hydrated salt moisture and polygonal pattern dynamics of salt crusts. We do this through three targeted experiments and identify for the first time how dynamic these surfaces are on a fine spatial and temporal scale (mm/hr). Initially (Experiment 1) we examine nocturnal moisture changes on a crust with a mix of ridged and continuous sections over a 39 day period using infra-red (IR) imagery and determine the change in elevation at this site over the same period using TLS. Next, (Experiment 2) we use TLS to examine the relationship between topographic and moisture change for different crusted surfaces during the night and, finally, (Experiment 3) we determine how the crust dries at dawn, again using TLS. For each crust type we relate differences in moisture and topographic change to distinct temperature and relative humidity conditions; which are in turn used to infer geochemical and thermodynamic processes occurring in surface and groundwater within the critical zone. We limit our study to nocturnal and early morning changes because this is when evaporation rates are suppressed and the surface has the potential to remain moist through fluxes via subsurface capillary or atmospheric condensation mechanisms (Groeneveld et al., 2010; Kinsman, 1976; Sturman and McGowan, 2009; Thorburn et al., 1992) for a sufficient time and magnitude that can be detected by IR camera and TLS (Nield et al., 2011; Nield et al., 2014).

Study Site

Field experiments were conducted on Sua Pan, Botswana (site location is centred at 20.5754°S, 25.959°E; See Figure 2) during the dry season in August, 2011 and August and September 2012. Sua Pan is a 3400 km^2 wet terminal discharge playa (Rosen, 1994) with a predominantly trona [$Na_3H(CO_3)_2{:}2H_2O$], halite [NaCl] and thenardite[Na_2SO_4] crust (Eckardt et al., 2008; Vickery, 2014) and is part of the Makgadikgadi Pan complex; one of the southern hemisphere’s largest aeolian dust source areas (Prospero et al., 2002; Vickery et al., 2013; Washington et al., 2003; Zender and Kwon, 2005). Sua Pan periodically floods during the summer but the surface remains dry for most of the year (Bryant *et al.,* 2007), with groundwater depths typically in the range 0.5-3.0 m over much of the pan (Eckardt et al., 2008). During the winter on Sua Pan, the mean climatic conditions include temperatures ranges of 9.6˚C to 29.3˚C and 13.3˚C to 32.9˚C in August and September respectively and mean monthly rainfall is 0.3 mm and 4.7 mm respectively. The pan is covered by a polygonal salt crust with spatially varying topographic characteristics (Nield et al., 2015; Nield et al., 2013b). Measurements for each experiment were collected at sites with three distinct crust types: (1) **R**idged, (2) **C**ontinuous and (3) **M**ixed (Figure 1). **R**idged surfaces consisted of well-formed, widely spaced, deep polygon ridges with some evidence of degradation and cracks within ridge surfaces and were composed of trona, halite and thenardite (Vickery, 2014). The **C**ontinuous sites were dominated by flat crust with occasional small, closed ridges and were predominantly composed of thenardite, with some mirabilite, halite and trona (Vickery, 2014). **M**ixed sites contained more irregular surface crust patterns, predominantly continuous and flat but with some notable disconnected ridged portions.

Methods

Time-lapse camera data collection and processing

Experiment 1 investigated the relationship between nocturnal moisture and climatic conditions using temporal series of LTL Acorn 5211A time-lapse camera images collected during 39 nights. A mixed surface (M1) was targeted to compare the response of ridged and continuous surfaces simultaneously with the same external climatic forcing. The camera was placed at a height of 1.5 m above the crust and programmed to record images every ten minutes with a resolution of 5 mega-pixels. The camera recorded true colour images passively during daylight and switched to active infra-red (IR) flash mode once its light sensor detected darkness (Figure 3). The photo sequences were post-processed to determine when the IR flash was used and a sequence of photos for each night were extracted between 1 hour after darkness and 30 minutes before sunrise to exclude any residual sunlight interference with the imagery. Surface moisture on or near (e.g. moisture within the top mm of the crust or water vapour derived from the crust) was then inferred from these IR photo sequences. The IR flash on the camera was 940 nm which is ideal for moisture detection because it is close to a key interstitial moisture absorption band for soils and sediments (Clark *et al.*, 2007), and so lower digital numbers (DN; akin to reflectance factor) within an IR image were likely to correspond to higher moisture within the top few mm of the crust.

Atmospheric conditions can also influence general reflectivity collected by this sort of imaging sensor, and so careful normalisation of crust reflectance values was undertaken using a standard grey calibration tile (15 x 15 cm) that was placed within the camera field-of-view on the surface of the crust. Similar links to decreased reflectance in response to higher pore moisture, or from minerals with greater structural or absorbed water, have been made in larger scale remote sensing of sodic playas by Mees et al. (2011). We therefore calculated mean DN values of 100 x100 pixel squares in each IR image for a) the calibration tile, b) a ridged crust and c) a continuous crust. The two crust sections were adjacent to each other and within the centre of the camera field-of-view (Figure 3). Mean values for the crust sections were then normalised using the calibration tile value for each individual image. We refer to this ratio as the dimensionless DN ratio (DNR). A DNR time-series collected in this manner gave us a non-invasive time-dependant index of surface absorption of the active infra-red light source; and is used here to infer variability in surface moisture with the playa salt crust. Further active IR measurements were collected in a similar manner using this approach at ridged (R3), mixed (M2) and continuous (C3) sites over a single night to enable a comparison of the IR and TLS relative moisture methods. DNR values were calculated in the same manner, using a calibration tile and a single 100 x 100 pixel crust section in the centre of the camera field-of-view.

TLS data collection and processing

Experiment 1 was complemented by TLS measurement of surface change over the same 39 night period. Crust topography was characterised on a) night 1 and b) night 39 using a time-of-flight Leica Scanstation. The TLS was placed at a height of 2.3 m and undertook a 360° scan overnight with a specified resolution of 5 mm at 30 m distance. A 10 x 10 m section of points were extracted from registered scans for each of the two nights (mean registration error 1 mm). Elevation points were gridded using mean values and 1 cm spacing, and empty cells were interpolated in MATLAB (Mathworks Inc) using the natural neighbour method and the surfaces were differenced to determine total change.

TLS return signal intensity (532 nm) has been documented as a useful tool for examining surface moisture on sand, particularly within a range 0 to 4 % gravimetric moisture content (Kaasalainen et al., 2008; Nield et al., 2011) and salt crusts, including surfaces sprayed with up to 800 ml/m^2 (Nield *et al.*, 2014). TLS is ideal for measuring changes in moisture on the playa surface, as it indicates the relative moisture of the crust at the surface (sub-mm), which is important for dust emission thresholds, rather than a depth averaged measurement as typically recorded by theta probes (Edwards *et al.*, 2013). We indicate relative moisture change by normalising the nocturnal return signal intensity by daytime values on the same surface following the methods of Nield et al. (2014). This comparison excludes any influence of distance (metres) on intensity values (Burton et al., 2011; Nield et al., 2013a; Nield et al., 2014) because each nocturnal value is normalised by the coincident value measured at the site during the previous day. Lower ratio values indicate an increase in moisture on the crust because more of the TLS signal has been absorbed.

In experiment 2 we use both the elevation and relative moisture capabilities of the TLS to extend experiment 1 and link nocturnal changes in moisture to changes in crust topography. We investigated two ridged (R1, R2) and two continuous (C1, C2) crust surfaces to explore the crust topography-moisture change relationship under different climate conditions. For experiment 2 nocturnal surface changes were assessed using four coincident 1 m x 2 m sections of crust (Figure 4). Initial scans of these four areas were undertaken during the day (before 16:40, scan times indicated in Table 1) to determine the daytime surface topography and surface dryness. These small pre-nocturnal scan sections took approximately 5 minutes to acquire, had an average point density of 34,500 points/m^2, and were located at a Euclidean distance of approximately 12.2 m from the scanner location and approximately 90° from each other. During the 360° nocturnal scan, three of these areas were rescanned overnight and the final area was rescanned after sunrise (Figure 4; see Table 1 for scan, sunset and sunrise times). These co-located repeat scan sections were then used to determine overnight and post-nocturnal net topographic change using the same topographic methods as experiment 1. Relative moisture change was determined from the same TLS point measurements over these co-located repeat scan sections following the methodology of Nield et al. (2014) and outlined above. For TLS moisture ratios, average intensity values for each 1 cm^2 grid cell were smoothed using a 9 x 9 cm moving window to reduce the influence of mixed pixels due to the laser footprint size (Hofle and Pfeifer, 2007; Nield et al., 2011). The 360° scan values for each co-incident 1 cm^2 grid cell were then normalised using the daytime small section grid cell values to determine overnight and post-nocturnal relative moisture change and recovery.

In experiment 3 we explore the relationship between climatic conditions and crust drying at dawn when atmospheric temperatures increase. For this experiment, a small section of the same ridged crust (1 x 2 m) was scanned over a two day period when climate varied (R4, R5). TLS measurements of the surface were repeated hourly before (5:40) and after (6:40, 7:40) sunrise. This area was also located at a Euclidean distance of 12.2 m from the TLS. Changes in moisture were calculated using the same methods as experiment 2.

The TLS was unable to detect changes in topography or moisture during the day. Spatially coincident daytime scans at a ridged site measured during the same day had uninterpolated elevation differences of less than 3 mm which is within the error range estimated by Hodge *et al.* (2009) for repeat scans of stony surfaces. Relative TLS moisture ratios measured during the day on the same crust surface did not detect any moisture change.

At each site examined in experiments 2 and 3 (R1, R2, R4, R5, C1, C2), 12 m x 12 m sections of points were extracted from an overnight 360° scan and processed into surfaces using the same methods as experiment 1. Additional scans were also undertaken following the same collection and processing methods as experiment 2 at a mixed (M2) and ridged (R3) site to enable a comparison of TLS and IR camera relative moisture calculations. Ridge width and spacing was calculated for all surfaces measured by TLS using the zero-up- and down-crossing method (Goda, 2000) to identify individual ridge units on 1 cm resolution transects, following the methods of Nield *et al.* (2013b).

Near-surface and sub-surface climate and geochemistry

TLS and camera data were supplemented with a range of additional meteorological measurements pertinent to examining atmospheric surface and subsurface feedbacks. Temperature and relative humidity were measured every ten minutes below the crust during experiments 1 and 2 using DS1923 iButtons (Maxim Integrated). These were inserted at each site approximately 1 cm beneath the crust at least two weeks before measurements commenced and several metres away from the section of crust being measured with the TLS to minimise any crust disturbance. An additional iButton was placed directly on top of the crust in a flat section for the experiment 3. Temperature and relative humidity at 1 m above the surface were also recorded every 10 minutes throughout the experiments in the centre of the study area using a CS215 (Campbell Scientific, Inc) temperature and relative humidity probe, housed in a radiation shield. Delta T theta probes recorded gravimetric moisture content integrated over a depth of 2 cm from the surface. Theta probe measurements were averaged to indicate daily mean values.

Across the field site, shallow groundwater samples were collected to investigate the geochemistry of natural water within the capillary/critical zone. Using a sterile pump sampler, water samples were extracted from pre-installed dip-wells. Groundwater depths ranged from 0.5-1.3m across the study area. In situ measurements of water temperature and pH were obtained at the time of sample collection. Samples were then immediately sealed, bagged in a light-tight container and were returned to the laboratory for analyses with minimal change in sample temperature. Once in the laboratory, standard methods were used to derive major cation and anion species (see Eckardt et al., 2008). As Benavente et al., (2015) outline, salt precipitation in a solution can occur through (i) changes in relative humidity (to reach the RH_{eq}), (ii) changes (often reduction) in temperature which can invoke changes in mineral solubility, and (iii) via dissolution of lower hydrated forms and the precipitation of the hydrated salts through changes in thermodynamic conditions. We provide here simulations of key components of these processes, using PHREEQC version 3.2 (Parkhurst and Appelo, 1999) with the Pitzer Database (Bryant et al., 1994) in order to characterise the stability and presence of likely mineral phases from the Na_2SO_4-H_2O and Na_2CO_3-H_2O systems under a range of recorded surface conditions.

Crust and underlying sediment samples were also analysed for bulk salt content. Surface sediment samples were sealed in bags and returned to the laboratory where soluble salts were removed using a standard rinse treatment with distilled water to determine the percentage mass of soluble salts present.

Results

Crust samples from the centre of the study site in 2011 had up to 82 % soluble salt by mass, whilst the underlying sediment contained up to 51 % soluble salt. In 2012 soluble salts by mass ranged from 57.7 to 76.9 % on the crust surface (Table 1). Generally, samples of shallow groundwater water displayed a pH > 9, and had high conductivity values (> 300,000 µS/cm). Analysis of mineral saturation data via PHREEQC (Bryant et al., 1994) suggest that typical shallow groundwater at our sites sampled at temperatures of between 20^{o}C and 25^{o}C were readily able to precipitate (i.e. were either saturated or supersaturated with respect to) a range of key Na_2SO_4-H_2O and Na_2CO_3-H_2O evaporite phases (Table 2 (a)).

Using PHREEQ we were able to determine key mineral components within our groundwater samples. At in situ daytime sample temperatures of between 20C and 25C, groundwater samples were generally saturated with respect to $CaCO_3$ phases (Calcite, Dolomite, Huntite) and undersaturated with regard to both Na_2SO_4-H_20 (thenardite, mirabilite) and Na_2CO_3-H_2O (Natron, Trona, Nacholite) phases. However some samples were initially saturated with regard to Nacholite ($NaHCO_3$) Pirssonite ($Na_2Ca(CO_3)_2$:$2H_2O$) and Gaylussite $CaNa_2(CO_3)_2$:$5H_2O$; suggesting that these phases could be present at the groundwater interface. Given these data, we were then able to simulate changes in mineral saturation within the samples as temperatures were either lowered or raised (i.e. from 0°C to 60°C) without further evaporation. In the first instance (Table 2), we found that as temperatures tended towards 0°C, mirabilite consistently reached super-saturation, Nacholite became under-saturated, and Pirssonite/Gaylussite were unaffected. Thereafter, as the temperatures were increased above 30°C (Table 2 (b)) we observed supersaturation with respect to Trona and Nacholite.

For each sample, we were able to use PHREEQ to forward-model the evaporation process in order to chart the precipitation (expressed as a molar yield) of likely key evaporite phases as the groundwater sample becomes concentrated over time; simulating the capillary rise and evolution of moisture as it moves to the surface. Given the importance of night-time temperature and RH, these experiments were undertaken at, 3°C, 8°C, 12°C, 20°C (Table 2 (c)). Importantly these data suggest that further evaporation of our samples at 20°C and above would yield a surface evaporite mineral assemblage of Thenardite and Trona with additional Pirssonite. As the temperature was systematically reduced to 3°C we found that the evaporite mineral assemblage changed to Halite, Mirabilite, Trona, and Pirssonite. The change in Mirabilite/Thenardite stability was observed to be apparent as the temperature dropped below 18°C. These experiments therefore highlight two key factors which can help us understand salt crust and moisture dynamics on our field site: (1) the confirmed presence of key Na_2SO_4-H_2O and Na_2CO_3-H_2O evaporite phases (Thenardite, Mirabilite, Trona, Pirssonite, with ancillary Halite), and (2) the likely hydration/dehydration of Mirabilite/Thenardite under observed conditions in the presence of moisture.

TLS topographic measurements show three distinct ridged, continuous and mixed surface patterns (Figure 5). Mean ridge heights and widths range from 0.018 m and 0.2 m on well-developed ridged surfaces, to 0.004 m and 0.08 m on continuous surfaces (Table 1).

TLS ratio and DNR measurements both indicate a similar synchronous variation in mean relative surface moisture for the different crust types ($R^2 = 0.98$; Figure 6). Co-incident theta probe moisture measurements integrated over the top 2 cm of each crust follow the same consistent trend as the TLS and DNR measurements and, specifically, the ridged surfaces are highlighted as being the driest and the continuous surfaces as the wettest. Surface or pore moisture also varied within each sample, with changes closely following the apparent topographic patterning. This was most noticeable on mixed and continuous crust examples (Figure 6c and 6e) where the inferred moisture had the greatest standard deviation.

Experiment 1: Changes in moisture on a mixed surface

During experiment 1 relative humidity and temperature at site M1 were inversely correlated (coefficient = -0.65), with high humidity and low temperatures experienced overnight (Figure 7 a). In general, the ridged area at M1 was drier than the continuous surface (Figure 7 b). However, on nights with high relative humidity (>70%; 14 occasions during the measurement period) the IR camera data showed that the DNR on the ridges dropped below the DNR observed on the continuous areas (approximately 1.4). During these periods when night-time relative humidity was high, the moisture of the continuous areas remained stable (9 occasions) or only increased by a small amount (<0.1), whereas a much larger increase (>0.28) in moisture was observed on the ridges. Importantly, this indicated that: (a) moisture on crust ridges fluctuated more than moisture on continuous crusted surfaces and (b) that ridged components of crusts were significantly more responsive to changes in atmospheric relative humidity. Mean overnight wind speeds during the measurement period varied from 0.68 m/s to 6.1 m/s, and did not appear to influence the responsiveness of the ridged surfaces (correlation coefficient = 0.09).

Interestingly, during experiment 1 the ridges on the mixed crust surface were seen to change significantly in both elevation and width (Figure 8); by as much as 1.5 mm/night on larger ridges. However, at the same time, continuous crusted areas remained relatively static (asymmetric distribution; mean elevation change = 0.187 mm/night; Figure 8c). This differential spatial trend in development in the ridged components of crusts is confirmed by a positive correlation between initial surface elevation and overall expansion (0.45; Figure 8d).

Experiment 2: Topographic and moisture change for different crusted surfaces

When observing ridged (R1, R2) and continuous (C1, C2) surfaces we can see that surface moisture within the crusts responded to climatic conditions in a similar way to the mixed surface (M1; experiment 1). Minimum temperature and maximum relative humidity values at 1 m above the surface varied during each of the four nocturnal study periods (R1, R2, C1, C2; Figure 9). Importantly, overnight surface temperatures at 1 m for an example of each crust type (R1, C2) were seen to drop below the 10°C threshold, that Saint-Amand *et al.* (1986) and Gillette *et al.* (2001) suggested was important for the salt phase switch from thenardite to mirabilite on Owens Lake. This period of low temperature also corresponded to an increased relative humidity at 1 m (> 60 %) indicative of a thenardite to mirabilite phase change. All of our relative humidity measurements were below 75 % which previous studies suggest is the minimum relative humidity required to observe overnight condensation on halite dominant crusts (Kinsman, 1976; Thorburn et al., 1992). Wind speeds were low and similar during each experiment (Table 1).

The morphology of the crust was observed to have a significant impact on sub-crust micrometeorology. At the ridged sites (R1, R2), cracks within the crust enabled the relative humidity below the crust on the ridged area to increase at a similar rate to that measured at 1 m above the surface (Figure 9). The subsequent decrease in relative humidity at dawn below the crust lagged behind the above crust relative humidity by an average of 1.5 hours. In contrast, the closed continuous crusts (C1, C2) maintained a high and stable sub-crust relative humidity throughout the experiment periods (Figure 9). This stability in relative humidity was irrespective of the conditions measured at 1 m height.

The nocturnal change in moisture in response to overnight decreases in temperature and increases in relative humidity was also seen to vary depending on crust type observed. In general, the ridged surfaces had a topographically controlled and spatially organised response (Figures 10 and 11). Overnight, ridged areas of crusts became progressively moister (elevation and TLS intensity ratio negatively correlated; Table 3), while continuous areas of crusts (between ridges) remained at, or close to, daytime moisture levels. The moistening of ridged areas was seen to be strongest during the night where high relative humidity conditions prevailed (correlation coefficient -0.63; Figure 11 R1). During the night with lower relative humidity (R2), the TLS only detected an increase in moisture on the upper sections of ridges (correlation coefficient -0.03; Figure 11 R2). Importantly, we observed that all crust surfaces quickly returned to typical daytime moisture values in the morning (9:00, 9:50 for R1 and R2 respectively); almost entirely replicating the same TLS intensity values as observed on the previous day.

Overnight change in surface elevation on the ridged surfaces was observed to vary depending on the prevailing atmospheric conditions (Figure 12). During the evening with high relative humidity

(Figure 12a R1), the continuous parts of the surface (between ridges) swelled by an average of 3 mm, whilst ridges either expanded or opened (mean coefficient for ridge areas and increased elevation = 0.21). Some isolated ridge sections changed their elevation by up to 30 mm; an order of magnitude higher than the continuous crusted areas. However, by 9.00 am, the continuous sections of crust had sunk back to their normal daytime elevation; but some ridge expansion remained. During the warmer, drier evening (Figure 12b R2), there was no detectable change in the continuous (inter-ridge) areas (mean elevation change less than 1 mm), but irreversible ridge expansion still occurred (maximum 8 mm).

Notably, the overnight moisture patterning of the continuous crusts was not correlated to topography (Figures 10 and 11; Table 3). Instead, small, isolated patches on the surface became moister overnight and returned to daytime values in the morning. The TLS measurements show that moistening was greater on the warmer, drier night (C1), and the surface dried more slowly on the cooler night (C2), when some moist patches were still measurable at 7:30am. There was minimal surface swelling overnight on the continuous surfaces (mean values ~2 mm), within the detection limits of the TLS and without spatial coherence. In contrast to the ridged surfaces the continuous surfaces returned to the same elevation as the previous day after sunrise.

Experiment 3: Early morning changes in moisture on a ridged surface

During the dawn drying experiment (3) the atmospheric relative humidity at 1 m above the crust was high on the first morning (maximum 83%; R4) and moderate on the second morning (maximum 70%; R5; Figure 13). During this experiment moisture was observed to be greatest on the ridged areas, while the continuous areas remained relatively constant (Figure 14). On the morning with high relative humidity (17th September 2012), the overall surface took longer to return to its daytime moisture levels; some ridges still indicated higher moisture levels 1.5 hours after sunrise. On the moderately humid morning (18th September) the majority of the surface had returned to daytime moisture levels 1.6 hours after sunrise. The IR camera (Figure 7b) on the mixed site (M1) demonstrated that on the night of the 16-17th September, the DNR of ridged surface dropped from 1.48 to 1.095, indicating a significant increase in moisture. IR camera DNR measurements during the night with moderate relative humidity (17-18th September) agree with TLS findings and show a smaller ridge moisture increase (DN ratio 1.48 to 1.145).

Atmospheric conditions, crust dynamics and the sodium sulphate phase diagram

Results from experiment 3 show how responsive crust dynamics can be to variable atmospheric conditions. During the drier (RH 70%) morning of the 18th (R5), the crust temperature/relative humidity temporal trajectories are close to, or within the thenardite stability zone of the thenardite-mirabilite phase diagram (Figure 13; Kracek, 1928; Steiger and Asmussen, 2008), while on the cooler, more humid morning of the 17th (R4), the first two measurements fall within the mirabilite stability zone. Given that the initial findings from geochemical modelling of groundwater also confirm that these phases are likely to be present under these conditions, we use this phase diagram as a proxy for the likelihood that the salts will absorb atmospheric and surface moisture when temperature and relative humidity are conducive to sodium sulphate mineral hydration (mirabilite formation). The phase diagram itself describes the stability thresholds for pure samples of thenardite and mirabilite. Thus, although we have shown that our crusts are more likely to be made up of intricate mixtures of sodium sulphate/carbonate evaporites and other minerals (clays, clastic, halite, etc), it is clear that the relative stability of these surfaces will still be governed by differential changes in atmospheric and surface temperature and humidity observed both within and above the surface crusts. Therefore, although the maximum relative humidity at 1 m above the surface for both nights was within the mirabilite stability zone (Kracek, 1928; Steiger and Asmussen, 2008), conditions remained in this zone for a much longer period on the 17th. By sunrise (6:08) on the 18th, the measurements at 1 m height were situated on the mirabilite-thenardite boundary, and measurements on the continuous surface were inside the thenardite stability zone (Kracek, 1928;

Steiger and Asmussen, 2008). On the 17th, both the 1 m and continuous surface measurements of temperature and humidity remained in the mirabilite stability zone until half an hour after sunrise (6:40 am), which agrees with similar observed magnitudes of the intensity TLS ratios for the 5:40 am and 6:40 am scans (Figure 14). On both days, measurements of temperature and relative humidity at 2 cm and 5 cm below the continuous crust remained inside the mirabilite stability zone. We therefore attribute crust dynamics at these sites to the relative diurnal hydration and dehydration of key sulphate bearing evaporite phases.

Importantly, the longer IR camera sequence from experiment 1 (M1) also follows a similar phase-shifting behaviour within the mirabilite/thenardite phase diagram (Figure 15). Maximum overnight relative humidity values were again within the mirabilite stability zone on the sodium sulphate phase diagram when the ridge DNR dropped below the continuous DNR. Further indicative evidence of moisture-flux was also apparent, as condensation was observed on the ridge crests in the early morning true-colour pictures during these exceedance periods (Figure 3d). Significantly, these observations agree with the Groeneveld *et al.* (2010) postulation that increased overnight moisture measured on the surface of Owens Lake was due to topographic control and atmospheric water condensing on the surface of ridges. Similar observations of surface moisture condensation on ridges overnight have been made by Sanchez-Moral et al. (2002). Together, our data provide the first direct evidence linking atmospheric conditions, spatially and temporally explicit salt crust dynamics and likelihood of sodium sulphate phase variability.

Feedbacks and implications of crust and moisture patterns

We have shown that the diurnal variation of moisture on a salt crust is linked to the crust topography (Figure 10; Table 3). These observed patterns may be controlled by a number of different micrometeorological, chemical, hydrological and physical processes and more data is required to explore the controls on surface pattern development. It is likely that the distinct pore-water-topography relationship may also enhance patterns in crust geochemistry at a similar micro-scale, and this leads us to further question this relationship. For example i) does the surface moisture patterning relate to changes in salt hydrology, or the condensation and evaporation of free water; and ii) does the elastic and inelastic expansion of the crust relate to salt phase changes and different capillary efficiency through variable pore spacing. Clearly, future studies are needed that combine detailed surface data with evaporation measurements (e.g. Groeneveld et al., 2010) and chemical analysis (e.g. spectroscopy, XRD and SEM; e.g. Drake, 1995; Buck et al., 2011;) to explore these intricate but important crust-geochemistry relationships. The crusts on Sua Pan are predominately fine grained and abiotic but in general variable physical (e.g. salt grain size and shape; Rad and Shokri, 2014; Singer et al., 2003) and microbiological (e.g. Acosta-Martinez et al., 2015; Rasuk et al., 2014; Viles, 2008) crust constituents also likely modulate or enhance surface pattern change by changing moisture absorption, crust elasticity, cohesion and porosity. Further, whilst our study highlights the complex behaviour of sodium sulphate rich salt crusts, more studies need to be conducted on geochemically diverse playas to determine the interplay of salts and clays in the construction of crust patterns.

Our data also emphasise that the development of different surface patterns over time is likely to be controlled by complex feedbacks between above and below-crust moisture transfers; fluxes which ultimately have the potential to modify salt chemistry and thereby influence topographic change rates and magnitudes . These environmental processes also exert fundamental and significant change on surface roughness (Nield et al., 2013) and likely pore connectivity (Nickling and Ecclestone, 1981) which can in turn alter atmospheric and subsurface moisture transfer rates respectively; and ultimately surface erodibility (Saint-Amand *et al.*, 1986) and evaporation rates (Groeneveld *et al.*, 2010).

Although the continuous surfaces that we monitored experienced some increase in moisture and minimal surface expansion overnight (Figure 11), this was patchy and likely controlled by heterogeneity within the geochemistry, pore spacing and topography (Eloukabi *et al.*, 2013). While the surface expansion was possibly a result of crystal growth either on or below the crust and potentially interactions with hygroscopic clay minerals, the elastic behaviour of these surfaces was notable. That they returned to their original topographic state at dawn, suggests that an initial phase of topographic perturbation may be needed to help induce crust expansion and thrusting. Surface perturbations could be internally driven, or the consequence of external disturbances including animals, motor vehicles, dust devils or thunderstorms. Ultimately the need for perturbation stimulus may account for the reduced rate of change measured on these flat, continuous and relatively homogeneous surfaces (Figure 8c) as they have a much reduced propensity to the range of possible feedbacks mentioned above. These findings agree with observations of moisture driven crust patterns made at a larger-scale (Nield *et al.*, 2015) and elucidate the importance of surface and atmospheric moisture fluxes in enhancing polygonal pressure ridge pattern development.

In terms of surface morphometric change, the observed thrusting of crust ridges agrees to some extent with the conceptual efflorescence and polygon thermal thrust model proposed by Krinsley (1970), particularly the assertion that maximum expansion occurs on the ridge crests. However, unlike the Krinsley model, we observed maximum expansion of ridges overnight, suggesting that differential salt efflorescence and surface hydration also play a role in crust surface expansion and contraction. Importantly, we find that the rapid rates of polygonal development (>30 mm/week) found by Nield et al. (2015) can occur in a single night on isolated crust sections given ideal temperature and relative humidity conditions (Figure 12a). This has significant implications for our understanding of changes in surface roughness (i.e. magnitude, rate, range) and represents a phase change in our understanding of the time-scales over which aerodynamic roughness and emission thresholds can change on surfaces that emit significant quantities of dust.

Conclusions

There is a complex relationship between patterns of surface topography and moisture response on sodic playas. Here we show the first high resolution (TLS) measurements of nocturnal complex surface change on a salt crust. Significantly, we identify temporal surface feedbacks between moisture and crust morphology to aid in our understanding of playa dust emissivity and evaporation variability.

Inelastic surface expansion is limited to ridged areas with higher topography, which also exhibit a temporary increase in moisture overnight. Continuous areas are less responsive to changes in atmospheric relative humidity, showing a reduced increase in non-spatially coherent moisture overnight and a slight, elastic increase in topography. These high resolution measurements of fast acting diurnal surface changes and the feedbacks both above and below the surface on moisture, potential sulphate salt phase and crust roughness, provide the first physical evidence of diurnal small-scale (mm) pattern changes on a dynamic, dust emitting playa and the ability of these moisture-pattern interactions to facilitate the development of polygonal ridges. Understanding how these ridges develop is important for accurately characterising surface roughness and evaporation rates which will enable the improvement of dust emission and evaporation model predictions.

Acknowledgements

This study was part funded by NERC as part of the DO4models project (NE/H021841/1), with travel support for Nield from a World University Network mobility grant and a University of Southampton SIRDF grant. Data processing was undertaken using the IRIDIS High Performance Computing Facility at the University of Southampton. K Vickery is thanked for excellent field discussions and helpful manuscript comments, EJ Milton, RT Wilson and G Roberts for valuable infra-red camera discussions and JA Gillies and WG Nickling for insightful discussions about relationships between our results and those from previous studies at Owens Lake. Anonymous reviewers and the ESPL editors are thanked for extensive comments on earlier versions of this manuscript that helped modify its direction. We thank the Botswana Ministry of Environment, Wildlife, and Tourism (permit EWT 8/36/4 XIV) and Botswana Ash (pty) Ltd for local support and access to the site.

References

Acosta-Martinez V, Van Pelt S, Moore-Kucera J, Baddock MC, Zobeck TM. 2015. Microbiology of wind-eroded sediments: Current knowledge and future research directions: *Aeolian Research*, **18**: 99-113.

Archer DJ, Wadge G. 2001. Modeling the backscatter response due to salt crust development: *IEEE Transactions on Geoscience and Remote Sensing*, **39**: 2307-2310.

Armesto-González J, Riveiro-Rodríguez B, González-Aguilera D, Rivas-Brea MT. 2010. Terrestrial laser scanning intensity data applied to damage detection for historical buildings: *Journal of Archaeological Science*, **37**: 3037-3047.

Baddock MC, Bullard JE, Bryant RG. 2009. Dust source identification using MODIS: A comparison of techniques applied to the Lake Eyre Basin, Australia: *Remote Sensing of Environment*, **113**: 1511-1528.

Benavente D, Brimblecombe P, Grossi CM. 2015. Thermodynamic calculations for the salt crystallisation damage in porous built heritage using PHREEQC: *Environmental Earth Sciences*, **74**: 2297-2313.

Benavente D, del Cura MAG, Garcia-Guinea J, Sanchez-Moral S, Ordonez S. 2004. Role of pore structure in salt crystallisation in unsaturated porous stone: *Journal of Crystal Growth*, **260**: 532-544.

Benavente D, Sanchez-Moral S, Fernandez-Cortes A, Canaveras JC, Elez J, Saiz-Jimenez C. 2011. Salt damage and microclimate in the Postumius Tomb, Roman Necropolis of Carmona, Spain: *Environmental Earth Sciences*, **63**: 1529-1543.

Bonython CW. 1956. The salt of Lake Eyre - its occurrence in Madigan Gulf and its possible origin: *Royal Society South Australia Transactions*, **79**: 66-92.

Briere PR. 2000. Playa, playa lake, sabkha: Proposed definitions for old terms: *Journal of Arid Environments*, **45**: 1-7.

Bryant RG, Bigg GR, Mahowald NM, Eckardt FD, Ross SG. 2007. Dust emission response to climate in southern Africa: *Journal of Geophysical Research-Atmospheres*, **112**: D09207.

Bryant RG, Rainey MP. 2002. Investigation of flood inundation on playas within the Zone of Chotts, using a time-series of AVHRR: *Remote Sensing of Environment*, **82**: 360-375.

Bryant RG, Sellwood BW, Millington AC, Drake NA. 1994. Marine-Like Potash Evaporite Formation on A Continental Playa - Case-Study from Chott-El-Djerid, Southern Tunisia: *Sedimentary Geology*, **90**: 269-291.

Bryant RG. 1999. Application of AVHRR to monitoring a climatically sensitive playa. case study: Chott El Djerid, Southern Tunisia: *Earth Surface Processes and Landforms*, **24**: 283-302.

Bryant RG. 2013. Recent advances in our understanding of dust source emission processes: *Progress in Physical Geography*, **37**: 397-421.

Buck BJ, King J, Etyemezian V. 2011. Effects of Salt Mineralogy on Dust Emissions, Salton Sea, California: *Soil Science Society of America Journal*, **75**: 1971-1985.

Buckley SJ, Howell JA, Enge HD, Kurz TH. 2008. Terrestrial laser scanning in geology: data acquisition, processing and accuracy considerations: *Journal of the Geological Society*, **165**: 625-638.

Bullard JE, Harrison SP, Baddock MC, Drake N, Gill TE, McTainsh G, Sun Y. 2011. Preferential dust sources: A geomorphological classification designed for use in global dust-cycle models: *Journal of Geophysical Research: Planets*, **116**: F04034.

Burrough SL, Thomas DSG, Singarayer JS. 2009. Late Quaternary hydrological dynamics in the Middle Kalahari: Forcing and feedbacks: *Earth-Science Reviews*, **96**: 313-326.

Burton D, Dunlap DB, Wood LJ, Flaig PP. 2011. Lidar Intensity as a Remote Sensor of Rock Properties: *Journal of Sedimentary Research*, **81**: 339-347.

Cahill TA, Gill TE, Reid JS, Gearhart EA, Gillette DA. 1996. Saltating particles, playa crusts and dust aerosols at Owens (dry) Lake, California: *Earth Surface Processes and Landforms*, **21**: 621-639.

Clark RN, Swayze GA, Wise R, Livo E, Hoefen T, Kokaly R, Sutley SJ. 2007. USGR digital spectral library splib06a, U.S. Geological Survey.

Darke I, Davidson-Arnott R, Ollerhead J. 2009. Measurement of Beach Surface Moisture Using Surface Brightness: *Journal of Coastal Research*, **25**: 248-256.

Darke I, Neuman CM. 2008. Field Study of Beach Water Content as a Guide to Wind Erosion Potential: *Journal of Coastal Research*, **24**: 1200-1208.

Darmenova K, Sokolik IN, Shao Y, Marticorena B, Bergametti G. 2009. Development of a physically based dust emission module within the Weather Research and Forecasting (WRF) model: Assessment of dust emission parameterizations and input parameters for source regions in Central and East Asia: *Journal of Geophysical Research: Atmospheres*, **114**: D14201.

Drake NA. 1995. Reflectance Spectra of Evaporite Minerals (400-2500-Nm) - Applications for Remote-Sensing: *International Journal of Remote Sensing*, **16**: 2555-2571.

Eckardt FD, Bryant RG, McCulloch G, Spiro B, Wood WW. 2008. The hydrochemistry of a semi-arid pan basin case study: Sua Pan, Makgadikgadi, Botswana: *Applied Geochemistry*, **23**: 1563-1580.

Edwards BL, Namikas SL, D'Sa EJ. 2013. Simple infrared techniques for measuring beach surface moisture: *Earth Surface Processes and Landforms*, **38**: 192-197.

Eloukabi H, Sghaier N, Ben Nasrallah S, Prat M. 2013. Experimental study of the effect of sodium chloride on drying of porous media: The crusty-patchy efflorescence transition: *International Journal of Heat and Mass Transfer*, **56**: 80-93.

Eugster HP, Jones BF. 1979. Behavior of major solutes during closed-basin brine evolution: *American Journal of Science*, **279**: 609-631.

Eugster HP, Smith GI. 1965. Mineral equilibria in the Searles Lake evaporites, California: *Journal of Petrology*, **6**: 473-522.

Genkinger S, Putnis A. 2007. Crystallisation of sodium sulfate: supersaturation and metastable phases: *Environmental Geology*, **52**: 295-303.

Gillette DA, Niemeyer TC, Helm PJ. 2001. Supply-limited horizontal sand drift at an ephemerally crusted, unvegetated saline playa: *Journal of Geophysical Research-Atmospheres*, **106**: 18085-18098.

Goda Y. 2000. Random seas and design of maritime structures: World Scientific.

Gran M, Carrera Js, Massana J, Saaltink MW, Olivella S, Ayora C, Lloret A. 2011. Dynamics of water vapor flux and water separation processes during evaporation from a salty dry soil: *Journal of Hydrology*, **396**: 215-220.

Groeneveld DP, Huntington JL, Barz DD. 2010. Floating brine crusts, reduction of evaporation and possible replacement of fresh water to control dust from Owens Lake bed, California: *Journal of Hydrology*, **392**: 211-218.

Grossi CM, Brimblecombe P, Menendez B, Benavente D, Harris I, Deque M. 2011. Climatology of salt transitions and implications for stone weathering: *Science of the Total Environment*, **409**: 2577-2585.

Haustein K, Washington R, King J, Wiggs G, Thomas DSG, Eckardt FD, Bryant RG, Menut L. 2015. Testing the performance of state-of-the-art dust emission schemes using DO4Models field data: *Geosci.Model Dev.*, **8**: 341-362.

Hodge R, Brasington J, Richards K. 2009. In situ characterization of grain-scale fluvial morphology using Terrestrial Laser Scanning: *Earth Surface Processes and Landforms*, **34**: 954-968.

Hofle B, Pfeifer N. 2007. Correction of laser scanning intensity data: Data and model-driven approaches: *ISPRS Journal of Photogrammetry and Remote Sensing*, **62**: 415-433.

Jentzsch PV, Ciobota V, Rosch P, Popp J. 2013. Reactions of Alkaline Minerals in the Atmosphere: *Angewandte Chemie International Edition*, **52**: 1410-1413.

Kaasalainen S, Kukko A, Lindroos T, Litkey P, Kaartinen H, Hyyppa J, Ahokas E. 2008. Brightness Measurements and Calibration With Airborne and Terrestrial Laser Scanners: *Geoscience and Remote Sensing, IEEE Transactions on*, **46**: 528-534.

Kampf SK, Tyler SW, Ortiz CA, Mu+¦oz JF, Adkins PL. 2005. Evaporation and land surface energy budget at the Salar de Atacama, Northern Chile: *Journal of Hydrology*, **310**: 236-252.

Kendall CGS, Warren JK. 1987. A review of the origin and setting of tepees and their associated fabrics: *Sedimentology*, **34**: 1007-1027.

King J, Etyemezian V, Sweeney M, Buck BJ, Nikolich G. 2011. Dust emission variability at the Salton Sea, California, USA: *Aeolian Research*, **3**: 67-79.

Kinsman DJJ. 1976. Evaporites; relative humidity control of primary mineral facies: *Journal of Sedimentary Research*, **46**: 273-279.

Kracek FC. 1928. International Critical Tables 3.

Krinsley DB. 1970. A Geomorphological and Paleoclimatological Study of the Playas of Iran. Part 1., Washington D.C., Geological Survey Reston VA, 356.

Lancaster N. 2004. Relations between aerodynamic and surface roughness in a hyper-arid cold desert: Mcmurdo dry valleys, Antarctica: *Earth Surface Processes and Landforms*, **29**: 853-867.

Legates DR, Mahmood R, Levia DF, DeLiberty TL, Quiring SM, Houser C, Nelson FE. 2011. Soil moisture: A central and unifying theme in physical geography: *Progress in Physical Geography*, **35**: 65-86.

Lichti D. 2005. Spectral Filtering and Classification of Terrestrial Laser Scanner Point Clouds: *The Photogrammetric Record*, **20**: 218-240.

Lorenz RD. 2011. Observations of wind ripple migration on an Egyptian seif dune using an inexpensive digital timelapse camera: *Aeolian Research*, **3**: 229-234.

Lorenz RD, Valdez A. 2011. Variable wind ripple migration at Great Sand Dunes National Park and Preserve, observed by timelapse imaging: *Geomorphology*, **133**: 1-10.

Lowenstein TK, Hardie LA. 1985. Criteria for the recognition of salt-pan evaporites: *Sedimentology*, **32**: 627-644.

MacKinnon DJ, Clow GD, Tigges RK, Reynolds RL, Chavez PS. 2004. Comparison of aerodynamically and model-derived roughness lengths (z(o)) over diverse surfaces, central Mojave Desert, California, USA: *Geomorphology*, **63**: 103-113.

Mahowald NM, Bryant RG, del Corral J, Steinberger L. 2003. Ephemeral lakes and desert dust sources: *Geophysical Research Letters*, **30**.

Marticorena B, Bergametti G. 1995. Modeling the atmospheric dust cycle: 1. Design of a soil-derived dust emission scheme: *Journal of Geophysical Research: Planets*, **100**: 16415-16430.

McKenna Neuman C, Langston G. 2006. Measurement of water content as a control of particle entrainment by wind: *Earth Surface Processes and Landforms*, **31**: 303-317.

Mees F, Castaneda C, Herrero J, Van Ranst E. 2011. Bloedite sedimentation in a seasonally dry saline lake (Salada Mediana, Spain): *Sedimentary Geology*, **238**: 106-115.

Nickling WG, Ecclestone M. 1981. The effects of soluble salts on the threshold shear velocity of fine sand: *Sedimentology*, **28**: 505-510.

Nickling WG. 1984. The stabilizing role of bonding agents on the entrainment of sediment by wind: *Sedimentology*, **31**: 111-117.

Nield JM, Bryant RG, Wiggs GFS, King J, Thomas DSG, Eckardt FD, Washington R. 2015. The dynamism of salt crust patterns on playas: *Geology*, **43**: 31-34.

Nield JM, Wiggs GFS. 2011. The application of terrestrial laser scanning to aeolian saltation cloud measurement and its response to changing surface moisture: *Earth Surface Processes and Landforms*, **36**: 273-278.

Nield JM, Wiggs GFS, Squirrell RS. 2011. Aeolian sand strip mobility and protodune development on a drying beach: examining surface moisture and surface roughness patterns measured by terrestrial laser scanning: *Earth Surface Processes and Landforms*, **36**: 513-522.

Nield JM, Chiverrell RC, Darby SE, Leyland J, Vircavs LH, Jacobs B. 2013a. Complex spatial feedbacks of tephra redistribution, ice melt and surface roughness modulate ablation on tephra covered glaciers: *Earth Surface Processes and Landforms*, **38**: 94-102.

Nield JM, King J, Jacobs B. 2014. Detecting surface moisture in aeolian environments using terrestrial laser scanning: *Aeolian Research*, **12**: 9-17.

Nield JM, King J, Wiggs GFS, Leyland J, Bryant RG, Chiverrell RC, Darby SE, Eckardt FD, Thomas DSG, Vircavs LH, Washington R. 2013b. Estimating aerodynamic roughness over complex surface terrain: *Journal of Geophysical Research: Atmospheres*, **118**: 2013JD020632.

Pakzad HR, Kulke H. 2007. Geomorphological features in the Gavkhoni playa lake, SE Esfahan, Iran: *Carbonates and Evaporites*, **22**: 1-5.

Parkhurst DL, Appelo CAJ. 1999. User's guide to PHREEQC (Version 2): A computer program for speciation, batch-reaction, one-dimensional transport, and inverse geochemical calculations: *U.S.Geological Survey Water Resources Investigations Report*, **99**: 310.

Peck AJ. 1960. The water table as affected by atmospheric pressure: *Journal of Geophysical Research*, **65**: 2383-2388.

Pelletier JD. 2006. Sensitivity of playa windblown-dust emissions to climatic and anthropogenic change: *Journal of Arid Environments*, **66**: 62-75.

Prospero JM, Ginoux P, Torres O, Nicholson SE, Gill TE. 2002. Environmental characterization of global sources of atmospheric soil dust identified with the Nimbus 7 Total Ozone Mapping Spectrometer (TOMS) absorbing aerosol product: *Reviews of Geophysics*, **40**: 2-1-2-31.

Rad MN, Shokri N. 2014. Effects of grain angularity on NaCl precipitation in porous media during evaporation: *Water Resources Research*, **50**: 9020-9030.

Rasuk MC, Kurth D, Flores MR, Contreras M, Novoa F, Poire D, Farias ME. 2014. Microbial Characterization of Microbial Ecosystems Associated to Evaporites Domes of Gypsum in Salar de Llamara in Atacama Desert: *Microbial Ecology*, **68**: 483-494.

Reeves CC. 1969. Lacustrine Structures: Depositional and Erosional, *Introduction to Paleolimnology*: Netherlands, Elsevier Science and Technology, -288.

Reynolds RL, Yount JC, Reheis M, Goldstein H, Chavez P, Fulton R, Whitney J, Fuller C, Forester RM. 2007. Dust emission from wet and dry playas in the Mojave desert, USA: *Earth Surface Processes and Landforms*, **32**: 1811-1827.

Rodriguez-Navarro C, Doehne E, Sebastian E. 2000. How does sodium sulfate crystallize? Implications for the decay and testing of building materials: *Cement and Concrete Research*, **30**: 1527-1534.

Rosen MR. 1994. The importance of groundwater in playas: a review of playa classifications and the sedimentology and hydrology of playas, *in* Rosen, M.R., ed., *Paleoclimate and Basin Evolution of Playa Systems, Geological Society of America Special Paper 289*: Boulder, CO, Geological Society of America, 1-18.

Saint-Amand P, Gaines C, Saint-Amand D. 1987. Owens Lake: an ionic soap opera staged on a natric playa, *Geological Society of America Centennial Field Guide - Cordilleran Section*: Boulder, CO, Geological Society of America, 145-150.

Saint-Amand P, Mathews LA, Gaines C, Reinking R. 1986. Dust storms from Owens and Mono Valleys, California, China Lake, CA, Naval Weapons Center Technical Publication Series 6731.

Sanchez-Moral S, Ordonez S, Benavente D, Garcia del Cura MA. 2002. The water balance equations in saline playa lakes: comparison between experimental and recent data from Quero Playa Lake (central Spain): *Sedimentary Geology*, **148**: 221-234.

Singer A, Zobeck T, Poberezsky L, Argaman E. 2003. The PM10 and PM2.5 dust generation potential of soils/sediments in the Southern Aral Sea Basin, Uzbekistan: *Journal of Arid Environments*, **54**: 705-728.

Steiger M, Asmussen S. 2008. Crystallization of sodium sulfate phases in porous materials: The phase diagram Na2SO4-H2O and the generation of stress: *Geochimica et Cosmochimica Acta*, **72**: 4291-4306.

Stoertz GE, Ericksen GE. 1974. Geology of Salars in Northern Chile: *U.S.Geological Survey Professional Paper*, **811**.

Sturman AP, McGowan HA. 2009. Observations of dry season surface energy exchanges over a desert clay pan, Queensland, Australia: *Journal of Arid Environments*, **73**: 74-81.

Thorburn PJ, Walker GR, Woods PH. 1992. Comparison of Diffuse Discharge from Shallow-Water Tables in Soils and Salt Flats: *Journal of Hydrology*, **136**: 253-274.

Tollerud HJ, Fantle MS. 2014. The temporal variability of centimeter-scale surface roughness in a playa dust source: Synthetic aperture radar investigation of playa surface dynamics: *Remote Sensing of Environment*, **154**: 285-297.

Tsui N, Flatt RJ, Scherer GW. 2003. Crystallization damage by sodium sulfate: *Journal of Cultural Heritage*, **4**: 109-115.

Turk LJ. 1975. Diurnal fluctuations of water tables induced by atmospheric pressure changes: *Journal of Hydrology*, **26**: 1-16.

Tyler SW, Kranz S, Parlange MB, Albertson J, Katul GG, Cochran GF, Lyles BA, Holder G. 1997. Estimation of groundwater evaporation and salt flux from Owens lake, California, USA: *Journal of Hydrology*, **200**: 110-135.

Tyler SW, Munoz JF, Wood WW. 2006. The response of playa and sabkha hydraulics and mineralogy to climate forcing: *Ground Water*, **44**: 329-338.

Vickery, K.J., 2014, A case study on dust supply from the Makgadikgadi Pans, Botswana [Doctor of Philosophy : University of Cape Town.

Vickery KJ, Eckardt FD, Bryant RG. 2013. A sub-basin scale dust plume source frequency inventory for southern Africa, 2005–2008: *Geophysical Research Letters*, **40**: 5274-5279.

Viles HA. 2008. Understanding Dryland Landscape Dynamics: Do Biological Crusts Hold the Key?: *Geography Compass*, **2**: 899-919.

Wadge G, Archer DJ. 2002. Remote measurement of the evaporation of groundwater from arid playas: *Proceedings of the Third International Symposium on Retrieval of Bio- and Geophysical Parameters from Sar Data for Land Applications*, **475**: 165-169.

Wadge G, Archer DJ. 2003. Evaporation of groundwater from arid playas measured by C-band SAR: *Geoscience and Remote Sensing, IEEE Transactions on*, **41**: 1641-1650.

Washington R, Todd M, Middleton NJ, Goudie AS. 2003. Dust-storm source areas determined by the total ozone monitoring spectrometer and surface observations: *Annals of the Association of American Geographers*, **93**: 297-313.

Washington R, Todd MC, Lizcano G, Tegen I, Flamant C, Koren I, Ginoux P, Engelstaedter S, Bristow CS, Zender CS, Goudie AS, Warren A, Prospero JM. 2006. Links between topography, wind, deflation, lakes and dust: The case of the Bodele Depression, Chad: *Geophysical Research Letters*, **33**.

Webb NP, Strong CL. 2011. Soil erodibility dynamics and its representation for wind erosion and dust emission models: *Aeolian Research*, **3**: 165-179.

Zehnder K, Schoch O. 2009. Efflorescence of mirabilite, epsomite and gypsum traced by automated monitoring on-site: *Journal of Cultural Heritage*, **10**: 319-330.

Zender CS, Kwon EY. 2005. Regional contrasts in dust emission responses to climate: *Journal of Geophysical Research-Atmospheres*, **110**: D13201.

Tables

Table 1 Site locations, descriptions and sample times.

Crust Type	Site Name	Location			Sample archive name	Sample Start Date	TLS Sample Times	Sunset on start date	Sunrise on following day	Bulk salt content (%)			Ridge Dimensions (m)					Temperature at 1 m above surface (°)			Relative Humidity at 1 m above surface (%)			Wind Speed at 1.68 m above surface (m/s)		
		Latitude (°S)	Longitude (°E)	Elevation (m)						Crust surface	Sediment immediately below crust	Subsurface sediment	Mean Height	Maximum Height	Height Standard Deviation	Mean Width	Mean Wavelength	Mean	Minimum	Maximum	Mean	Minimum	Maximum	Mean	Minimum	Maximum
Ridged	**R1**	20.6032	25.9301	910.79	D10	18/08/2011	15:30, 19:50, 00:05, 4:20, 9:00	18:03	6:35	-	-	-	0.018	0.067	0.011	0.200	0.316	15.07	5.57	26.96	46.81	17.19	70.87	2.40	0.29	8.27
	R2	20.6032	25.9301	910.79	D10	19/09/2012	16:00, 18:10, 22:00, 2:00, 9:50	18:11	6:07	-	-	-	0.012	0.089	0.010	0.131	0.214	23.01	9.34	36.81	34.29	14.46	58.32	2.13	0.16	7.53
	R3	20.6032	25.9301	910.79	D10	05/08/2012	-	17:59	6:43	60.1	45.5	32.3	0.012	0.080	0.010	0.135	0.218	17.39	7.76	29.65	36.53	17.93	58.90	2.88	0.03	8.25
	R4	20.5585	26.0071	909.76	L5	17/09/2012	5:40, 6:40, 7:40	18:11	6:09	-	-	-	0.018	0.070	0.010	0.161	0.292	19.30	9.72	29.30	49.82	19.23	84.80	2.93	0.03	9.65
	R5	20.5585	26.0071	909.76	L5	18/09/2012	5:30, 6:40, 7:50	18:11	6:08	-	-	-	0.018	0.070	0.010	0.161	0.292	20.73	9.34	34.95	40.95	16.19	78.97	2.23	0.28	6.49
Continuous	C1	20.6126	25.9876	909.95	J11	22/08/2011	13:15, 19:00, 23:15, 3:30, 7:45	18:04	6:32	-	-	-	0.004	0.021	0.003	0.080	0.128	19.16	10.77	32.75	30.10	11.23	53.23	3.85	0.78	10.26
	C2	20.5585	26.0071	909.76	L5	03/08/2012	16:00, 19:40, 3:30, 7:30	17:59	6:44	76.9	56.4	25.4	0.008	0.043	0.005	0.176	0.270	16.46	6.81	27.68	48.27	24.12	74.49	2.03	0.13	5.06
Mixed	**M1**	20.5760	25.9111	911.09	B7	02/08/2012	-	17:58	6:45	57.7	33.8	38.8	0.006	0.085	0.007	0.127	0.172	16.95	6.81	30.12	42.50	17.40	74.49	2.10	0.11	5.06
	M2	20.5493	25.9785	910.05	I4	04/08/2012	-	17:59	6:44	69.6	40.1	17.5	0.018	0.072	0.010	0.167	0.283	16.97	8.01	29.04	42.28	21.96	60.71	1.85	0.03	4.18

Table 2 (a) Typical geochemistry of groundwater samples taken from the study site.

Sample Code	Location		Water Table Depth	Cl	Br	SO_4	K	Na	Mg	Ca	Alkalinity	pH	Temperature	Conductivity (20C)
	Latitude (°S)	Longitude (°E)	cm	mg/l	mg/l	mg/l	mg/l	mg/l	mg/l	mg/l	mg/l		C	microS/cm
FR11-L5	20.5585	26.0071	52	94822.8	142.6	8659.2	3184.8	86512.3	3.4	16.4	39010.0	9.3	20.5	274738.0
FR11-I8	20.5936	25.978	74	120726.5	203.3	12812.5	3987.9	113005.0	2.8	13.5	51110.0	9.5	22.0	408267.0
FR11-G6	20.5754	25.959	121	116820.0	186.1	12575.5	4180.5	108220.7	3.5	10.8	48670.0	9.8	23.0	393631.0

Table 2 (b) Mineral saturation data for sample FR11-G6 with changes in temperature derived using PHREEQ.

Phase	Equation	0	5	10	15	20	25	30	35	40	45	50	Temperature (
Calcite	$CaCO_3$	2.56	2.62	2.67	2.72	2.78	2.83	2.88	2.93	2.98	3.02	3.07	
Dolomite	$CaMg(CO_3)_2$	4.22	4.33	4.43	4.53	4.62	4.71	4.8	4.88	4.96	5.03	5.1	
Gaylussite	$CaNa_2(CO_3)_2{:}5H_2O$	2.6	2.64	2.68	2.72	2.76	2.8	2.83	2.86	2.89	2.92	2.94	
Halite	NaCl	-0.17	-0.16	-0.16	-0.16	-0.16	-0.16	-0.16	-0.17	-0.17	-0.18	-0.18	
Huntite	$CaMg_3(CO_3)_4$	3.95	4.23	4.51	4.79	5.07	5.36	5.64	5.93	6.22	6.52	6.81	
Magnesite	$MgCO_3$	1.17	1.17	1.16	1.16	1.15	1.14	1.13	1.12	1.11	1.09	1.08	
Mirabilite	$Na_2SO_4{:}10H_2O$	0.16	-0.08	-0.31	-0.53	-0.74	-0.93	-1.12	-1.3	-1.46	-1.62	-1.76	
Nahcolite	$NaHCO_3$	-0.15	-0.07	-0.01	0.05	0.09	0.14	0.17	0.2	0.22	0.24	0.25	
Natron	$Na_2CO_3{:}10H_2O$	-0.89	-0.85	-0.81	-0.77	-0.74	-0.7	-0.67	-0.64	-0.61	-0.59	-0.56	
Pirssonite	$Na_2Ca(CO_3)_2{:}2H_2O$	2.75	2.8	2.84	2.88	2.92	2.96	2.99	3.02	3.05	3.08	3.1	
Thenardite	Na_2SO_4	-1.08	-0.98	-0.9	-0.83	-0.77	-0.71	-0.67	-0.63	-0.59	-0.56	-0.54	
Trona	$Na_3H(CO_3)_2{:}2H_2O$	-0.32	-0.2	-0.09	0.01	0.1	0.18	0.25	0.31	0.36	0.4	0.44	

Table 2 (c) Initial molar yield of key equilibrium mineral phases from sample FR11-i8 under evaporation at four different temperatures; derived using PHREEQ.

Phase	Equation	20	12	8	3	Temperature
	Moles in Assemblage					
Halite	NaCl	0.00	9.04	8.99	8.94	
Magnesite	$MgCO_3$	1.88	8.94	9.14	9.36	
Mirabilite	$Na_2SO_4{:}10H_2O$	0.00	19.53	19.78	19.96	
Nahcolite	$NaHCO_3$	0.00	0.00	0.00	0.00	
Natron	$Na_2CO_3{:}10H_2O$	0.00	0.00	0.00	0.00	
Pirssonite	$Na_2Ca(CO_3)_2{:}2H_2O$	11.88	18.94	19.14	19.36	
Thenardite	Na_2SO_4	15.08	0.00	0.00	0.00	
Trona	$Na_3H(CO_3)_2{:}2H_2O$	19.72	20.09	20.06	20.00	

Table 3 Correlation coefficients between surface elevation and intensity TLS ratio for ridged and continuous site overnight measurements. See Table 1 for actual times at each period.

	Time period	Surface			
		R1	R2	C1	C2
Correlation coefficient between elevation and intensity ratio	1	-0.18	0.12	0.23	0.04
	2	-0.63	-0.03	-0.05	nan
	3	-0.48	0.10	0.16	-0.07
	4	0.12	0.02	-0.10	-0.04

Figures

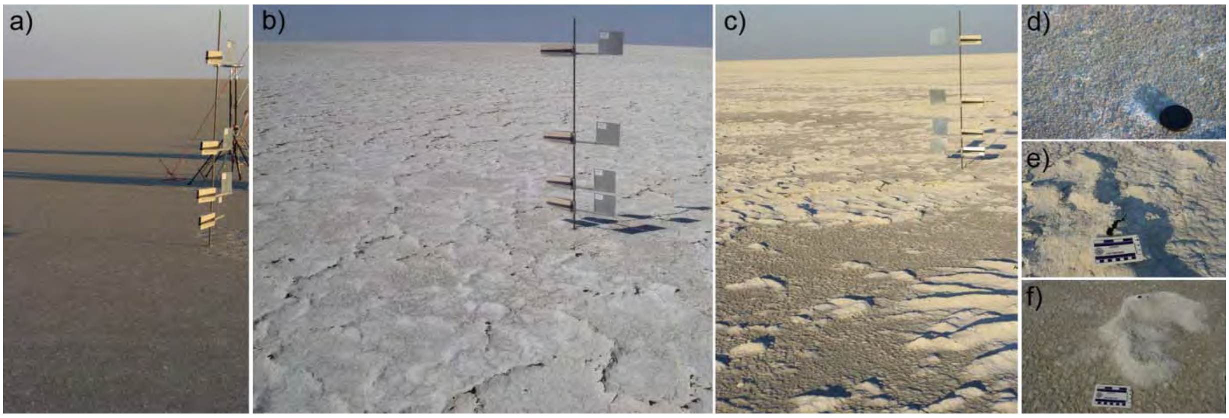

Figure 1 Examples of a) continuous, b) ridged and c) mixed salt crust surfaces on Sua Pan. Close-ups of each crust pattern are indicated in d-f respectively.

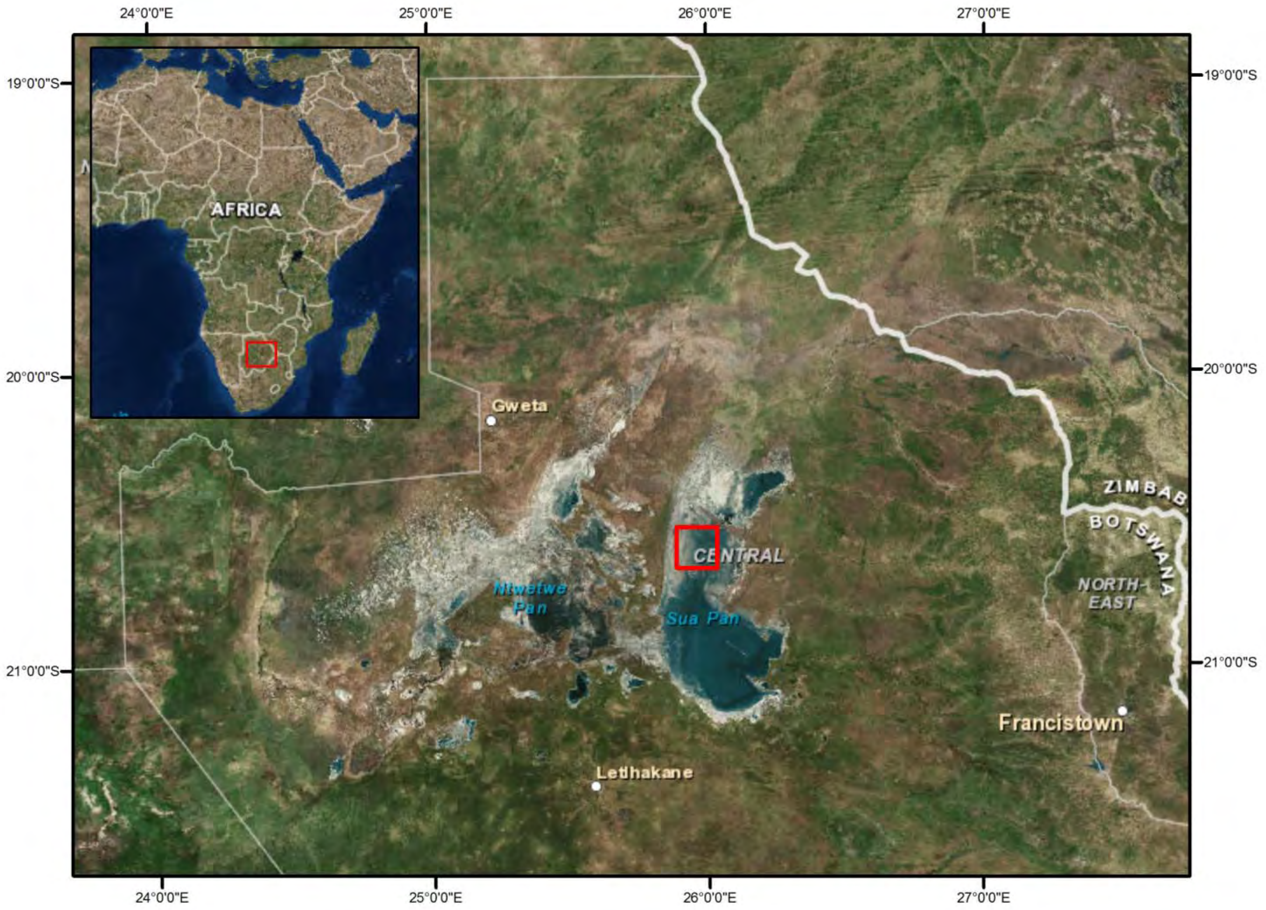

Service Layer Credits: Copyright:© 2013 Esri, DeLorme, NAVTEQ, TomTom
Source: Esri, DigitalGlobe, GeoEye, i-cubed, USDA, USGS, AEX, Getmapping, Aerogrid, IGN, IGP, swisstopo, and the GIS User Community

Figure 2 Location of Sua Pan in Botswana, upper left insert indicates location within Africa. Red box on main map indicates location of study sites.

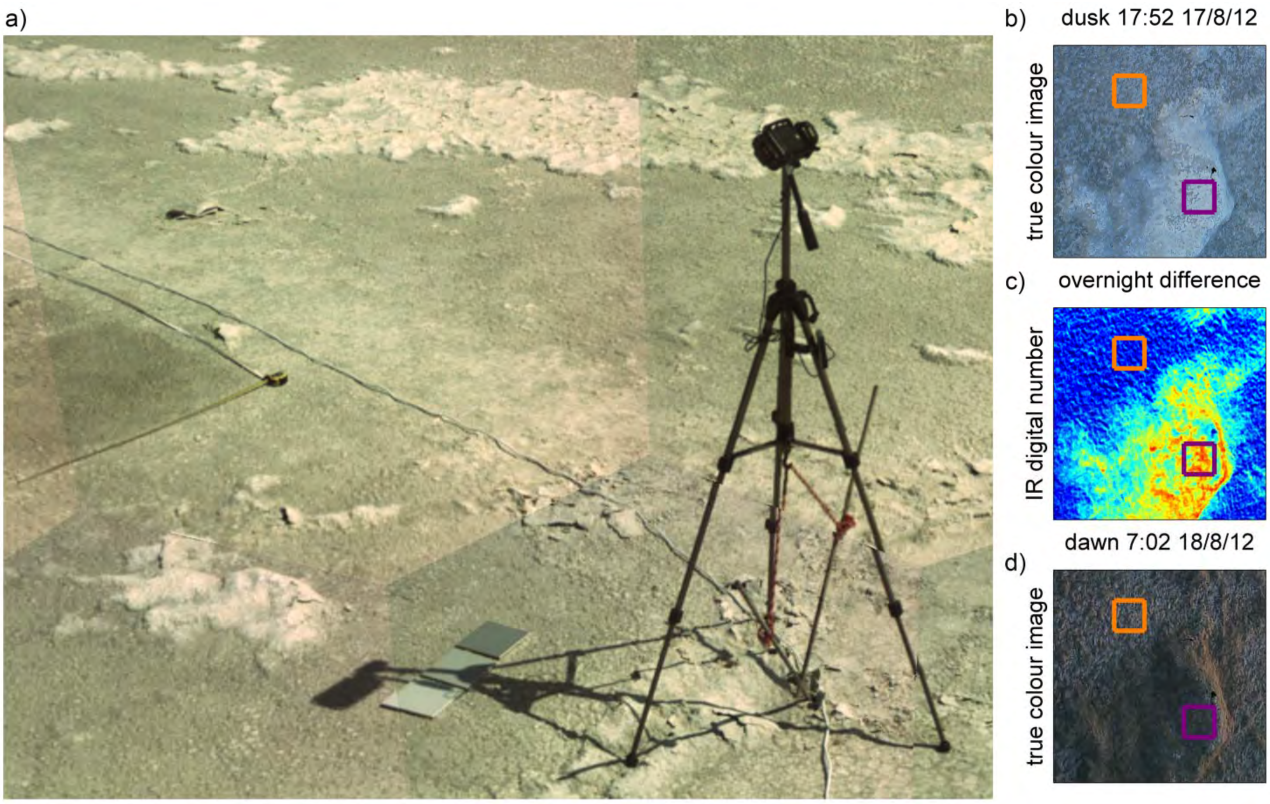

Figure 3 a) IR-camera set-up on a mixed (M1) surface, with calibration tiles positioned within the camera field of view. Tape on left side is 1 m. Right side are image sections (1000 x 1000 pixels) from the camera: b) true colour pre-sunset c) overnight infra-red digital number (DN) image, and d) true colour post-sunrise. Orange and purple boxed areas indicate pixels used to determine overnight change on continuous and ridged sections respectively (100 x 100 pixels).

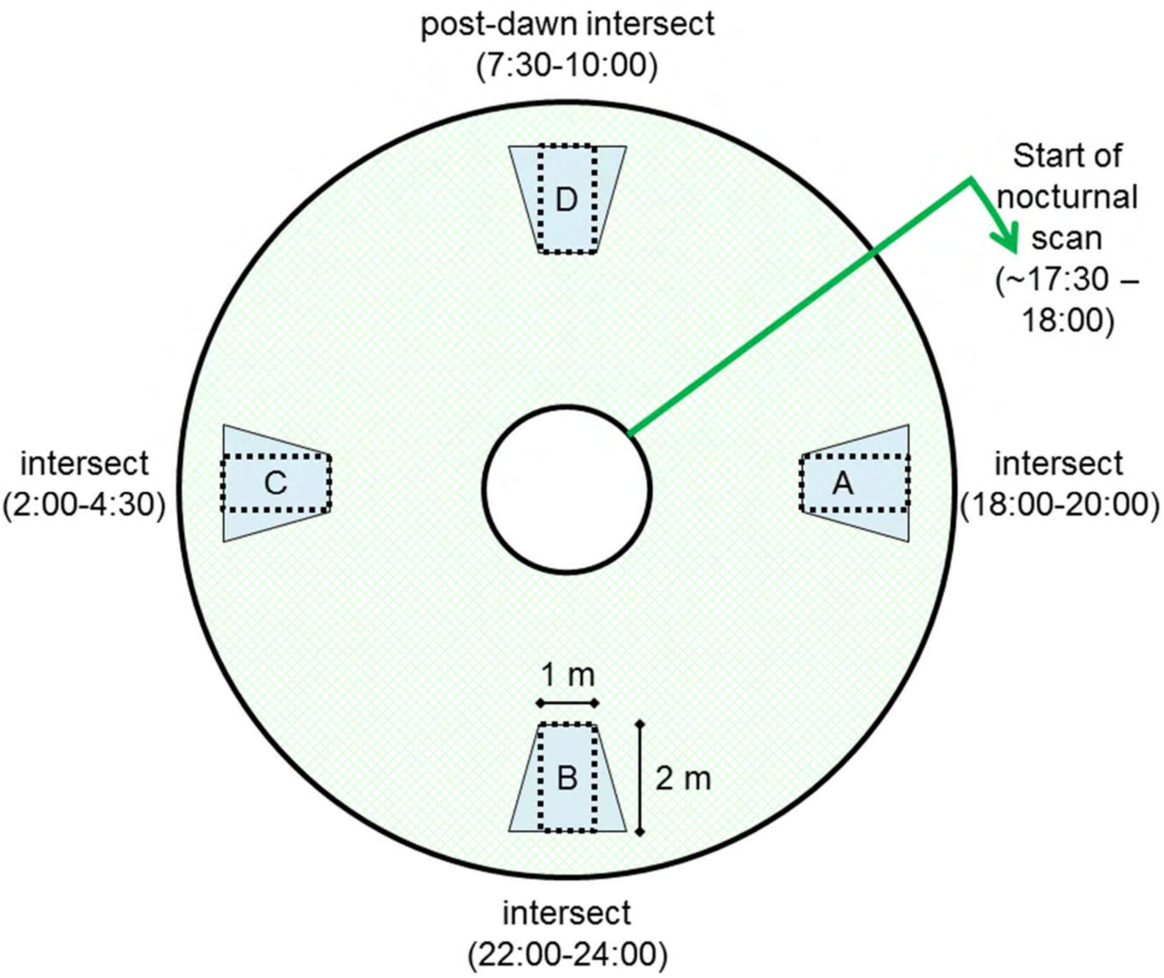

Figure 4 TLS set-up for Experiments 1 and 2. Solid segments (A, B, C, D) were scanned during daytime conditions prior to the start of the nocturnal scan. Nocturnal scan covered full 360° (cross-hatched donut) and was used to extract 10 x 10 m squares for ridge height and spacing calculations, as well as the temporal change for Experiment 1. Nocturnal scan start location, segment locations and times are approximate and were aligned to ensure representative, similar crust surfaces in A, B, C, D. 1 x 2 m rectangles were extracted during post processing to compare relative moisture and topography at A, B, C and D.

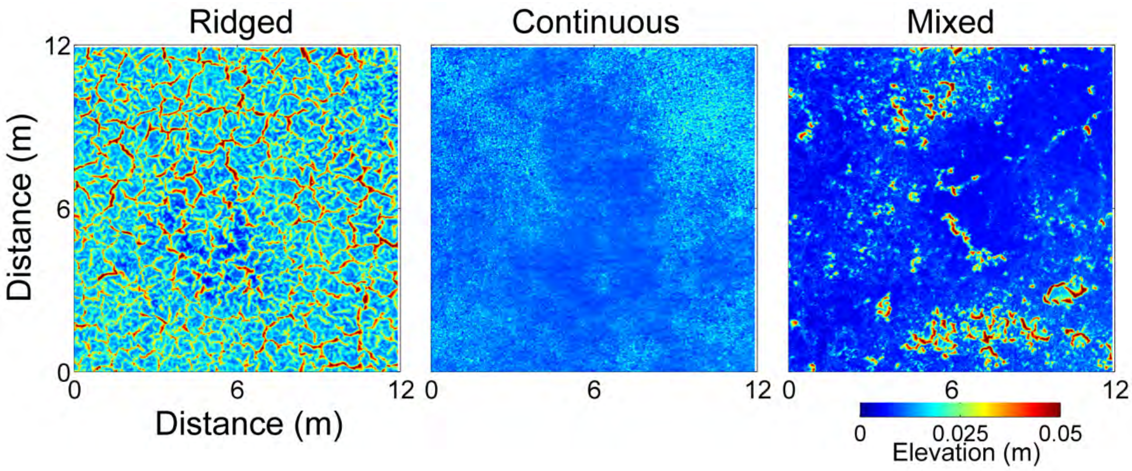

Figure 5 Surface elevations measured by TLS for representative 12 m x 12 m squares of each crust type (north at the top of each square).

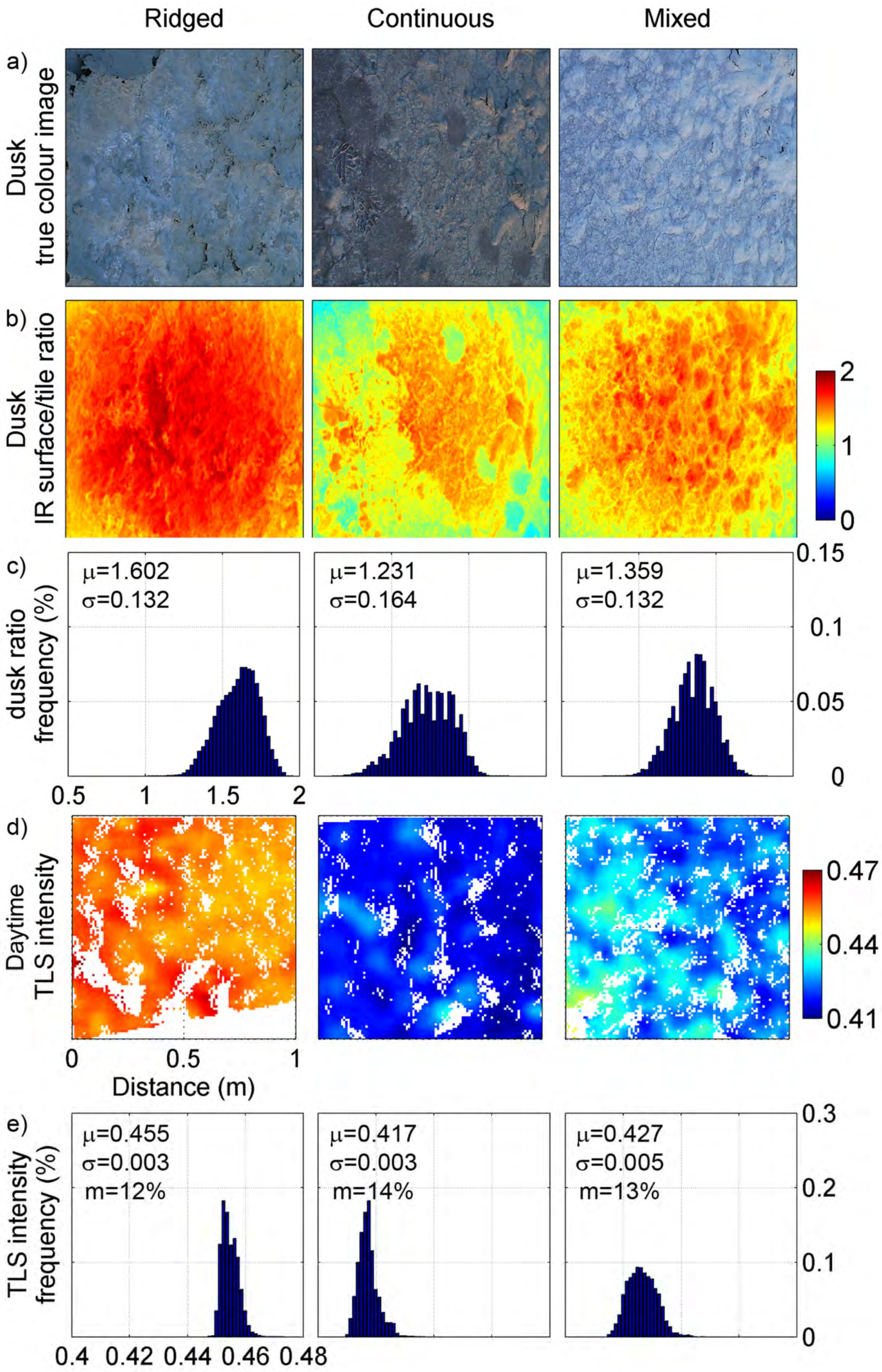
Ridged
Continuous
Mixed
a)
Dusk
true colour image
b)
Dusk
IR surface/tile ratio
2
1
0
c)
dusk ratio
frequency (%)
μ=1.602
σ=0.132
μ=1.231
σ=0.164
μ=1.359
σ=0.132
0.15
0.1
0.05
0
0.5
1
1.5
2
d)
Daytime
TLS intensity
0.47
0.44
0.41
0
0.5
1
Distance (m)
e)
TLS intensity
frequency (%)
μ=0.455
σ=0.003
m=12%
μ=0.417
σ=0.003
m=14%
μ=0.427
σ=0.005
m=13%
0.3
0.2
0.1
0
0.4
0.42
0.44
0.46
0.48

834

Figure 6 Camera and TLS single time measurements on ridged (R3), continuous (C2) and mixed (M2) surfaces, orientated with north at the top of each square. Mean and standard deviation values for histograms denoted by μ and σ respectively. Depth averaged (2 cm) gravimetric moisture content from theta probes indicated by m. a) True colour images taken with the time-lapse camera, half an hour before sunset. b) DNR of infra-red return signal and tile value for each site one hour after sunset, for the same area as a) (1000 x 1000 pixels). c) Histograms of DNR for each area in b). d) TLS return signal intensity corrected for distance, measured on a 1 x 1 m area during daylight on the same surface as a) but on a different area, approximately 12.2 m from the scanner head. e) Histograms of the TLS return signal intensity for each of the patches in d).

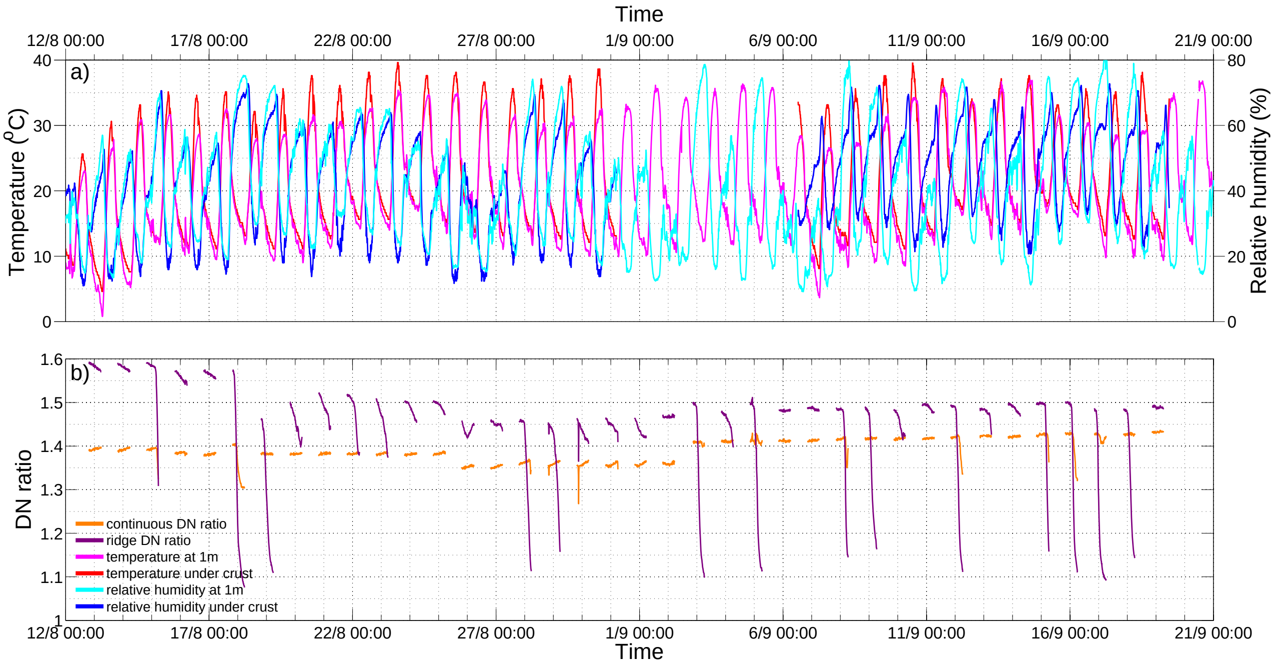

Figure 7 a) Temperature and relative humidity above and below the crust at M1 during August and September 2012. b) Nocturnal digital number (DN) ratios of ridged and continuous crust and calibration tile from infra-red (IR) flash camera.

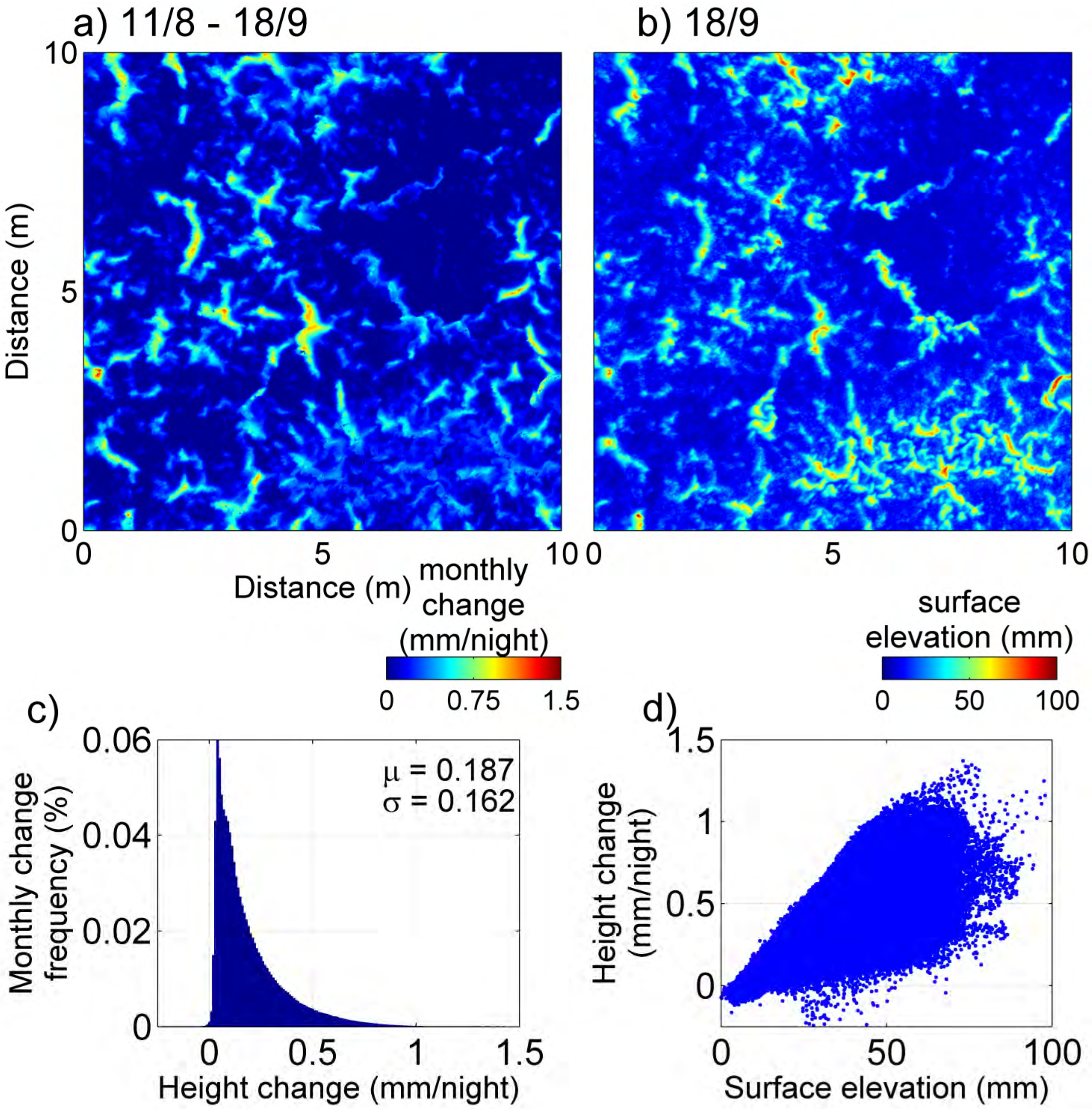

Figure 8 a) Nightly change in surface topography at mixed (M1) site between 11/8/12 and 18/9/12. b) Final surface elevation at M1 on 18/9/12. c) Histogram of elevation change per night between measurement periods. Mean and standard deviation values for histograms denoted by μ and σ respectively. d) Elevation change vs. final surface elevation.

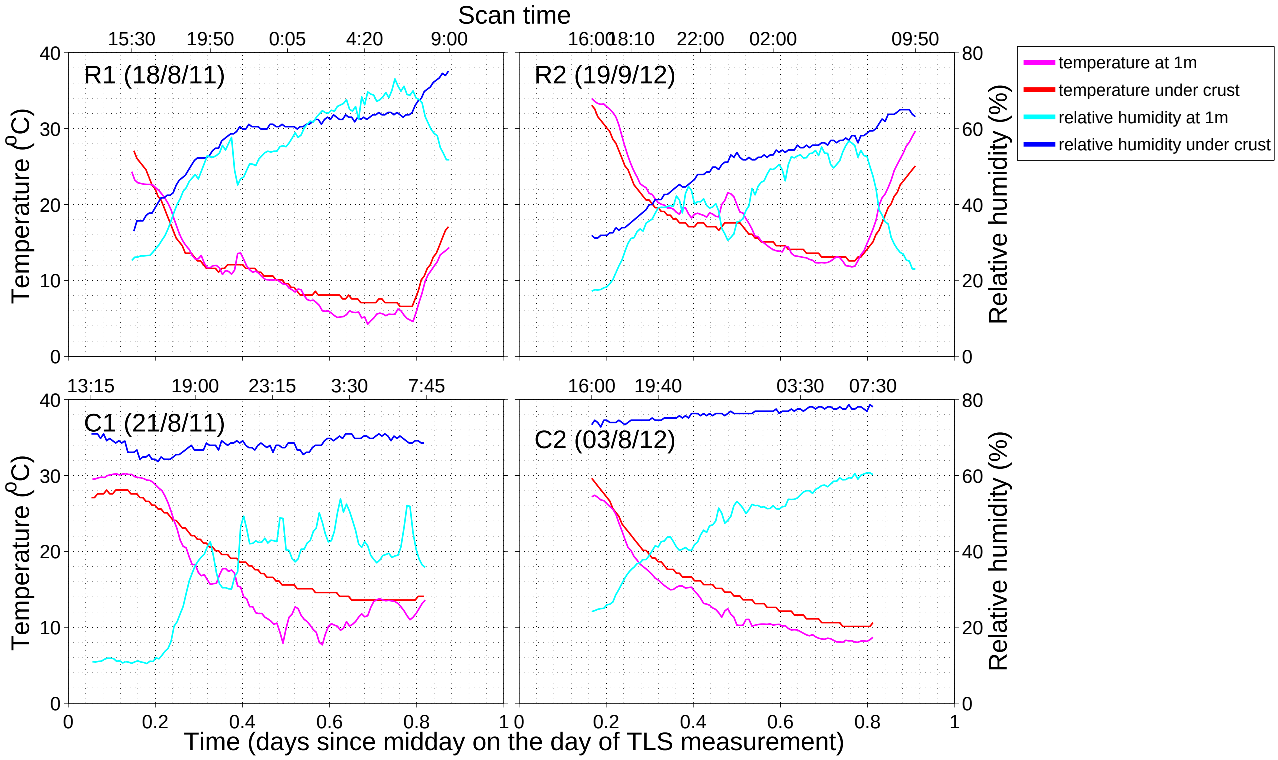

Figure 9 Overnight temperature and relative humidity above and below the crust for ridged (R1, R2) and continuous (C1, C2) surfaces during TLS scanning. Scan time relates to the times when repeat surface scans were undertaken to extract moisture and elevation data corresponding to the DEMs. Exact sunset and sunrise times are indicated in Table 1 (approximately 18:00 and 06:00).

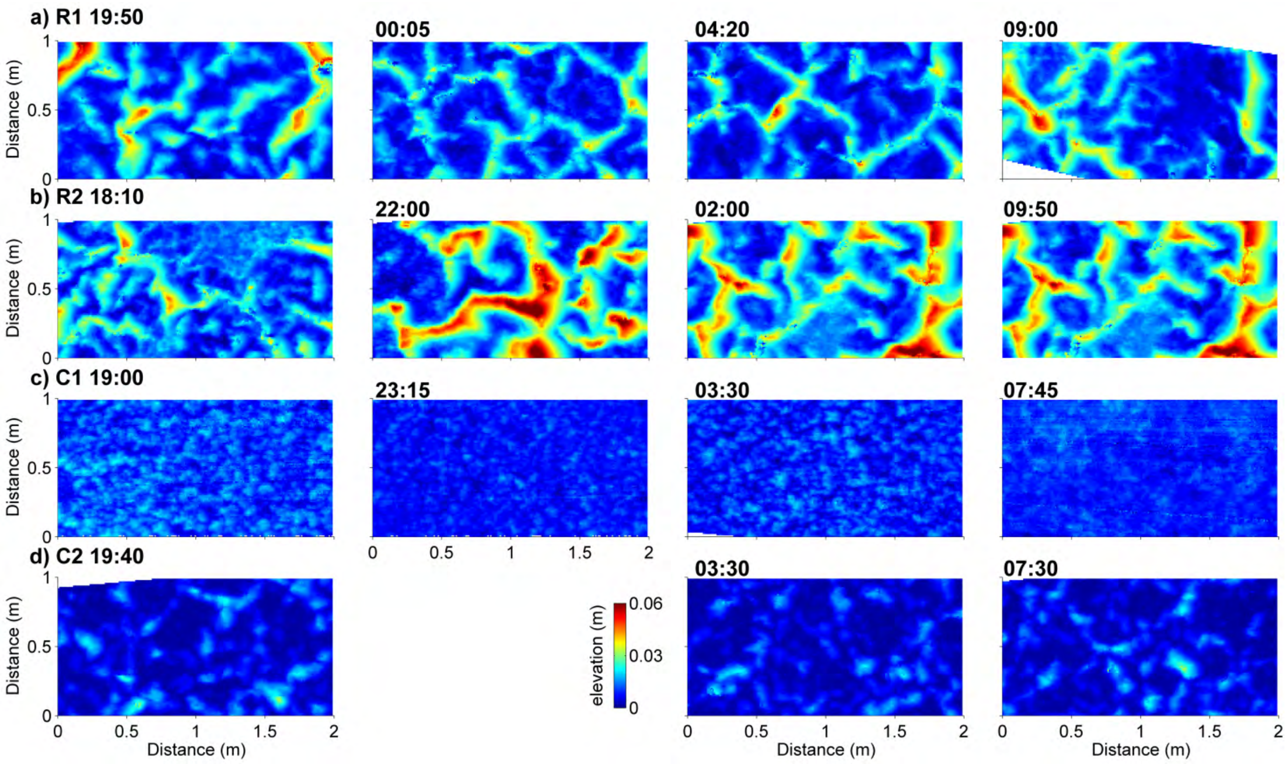

Figure 10 Surface elevations for each section of crust used to analyse nocturnal trends in moisture and elevation change. Red indicates ridges and blue flatter, continuous areas. The time each scan was collected is show above each plot. See Table 1 for more details on each set-up.

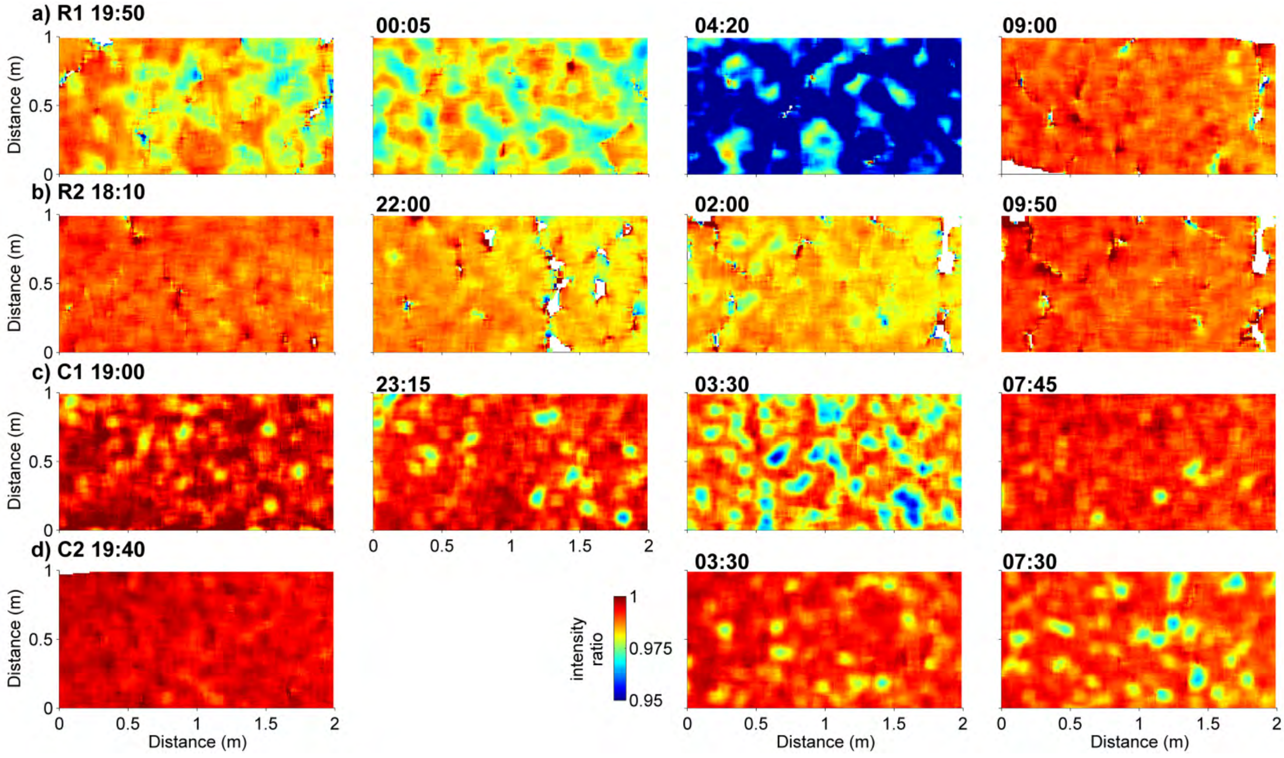

Figure 11 Nocturnal trends in surface moisture for each nocturnal crust section, coloured by the TLS ratio of the intensity of the surface during the night and day. Sunset and sunrise times are indicated in Table 1. Blue indicates a higher relative increase in moisture, red little change in moisture overnight. The time each scan was collected is shown above each plot. Corresponding climatic conditions and surface elevations are indicated in Figures 9 and 10 respectively.

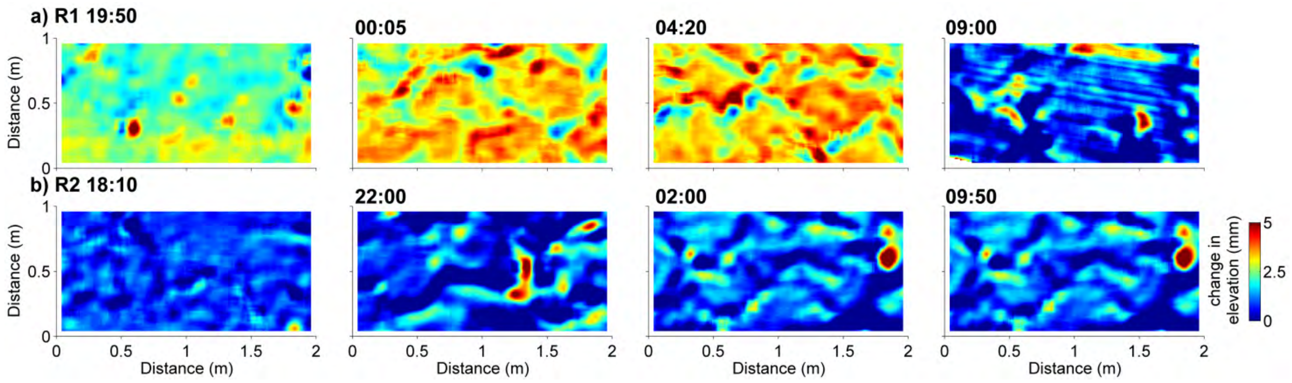

Figure 12 Nocturnal change in surface elevation from early evening (left) to after dawn (right) for R1 and R2. Sunset and sunrise times are indicated in Table 1. Plots correspond to the same areas shown in Figures 10 and 11, and are coloured by change between scanned topography overnight and the previous day. Red indicates surface expansion greater than 5 mm. Refer to Figure 9 for corresponding temperature and relative humidity.

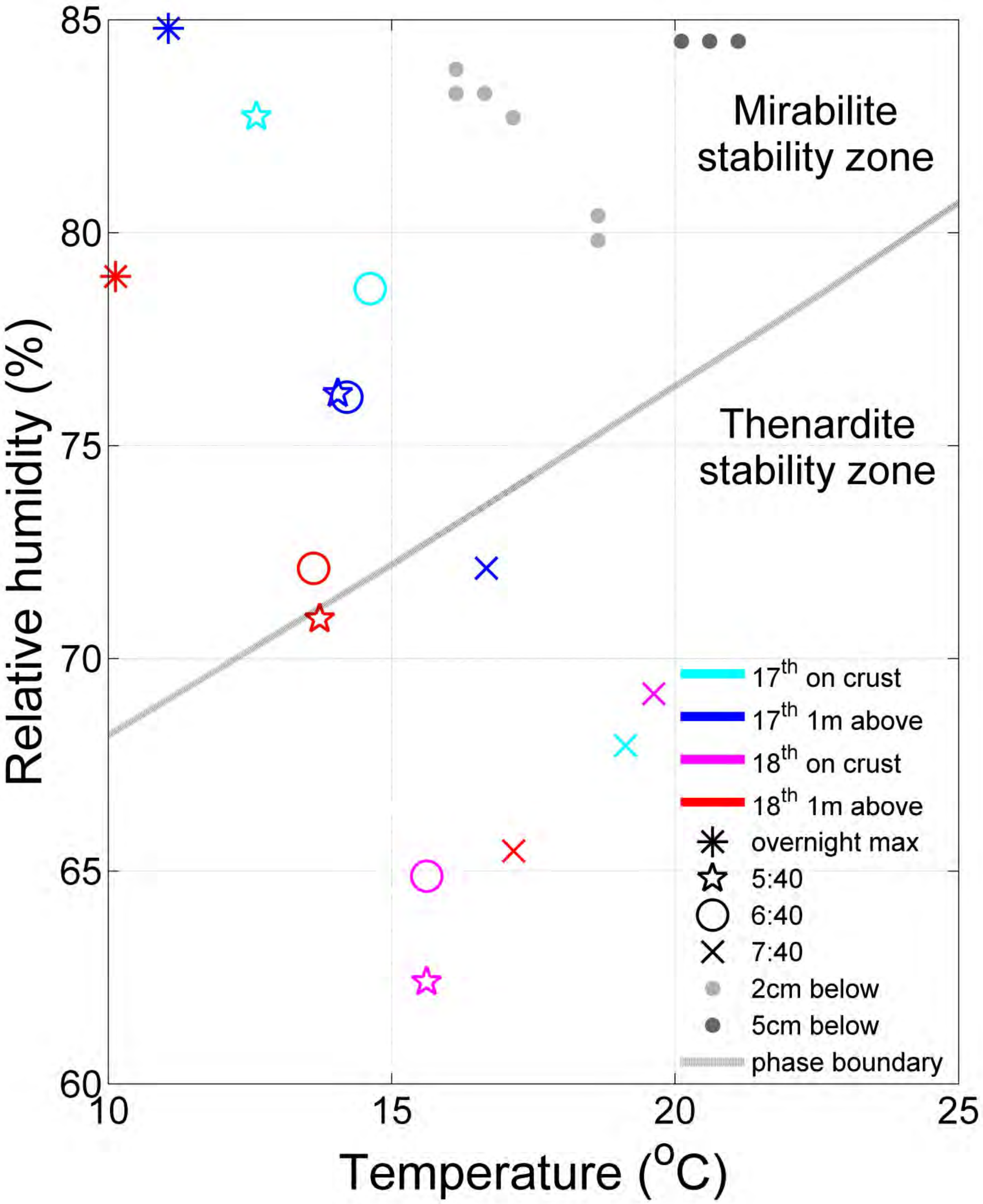

Figure 13 Early morning trajectories of temperature and relative humidity above, on and below the crust for each surface measurement at R4 and R5, indicating climate trajectory is more extreme under conditions on the 17th September 2012.

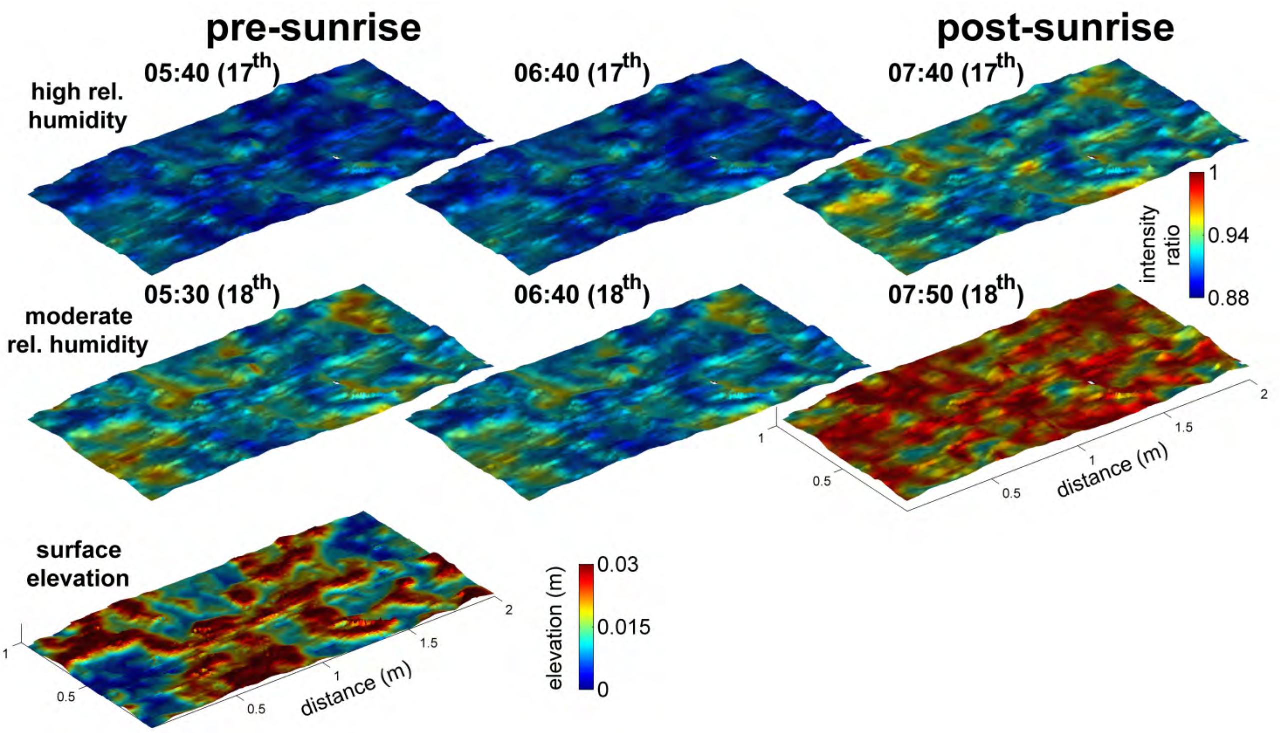

Figure 14 Ridged crust topography coloured by the early morning change in surface moisture (R4 and R5). Upper row (R4) shows increased relative wetting of ridged areas under high relative humidity (maximum 83%) and the surface takes longer to dry after dawn. Similar spatial response under moderate relative humidity (R5; middle row; maximum 70%), but faster drying after dawn. Sunrise was at 6:09 and 6:08 for the 17th and 18th respectively. Corresponding climate conditions are shown in Figure 13.

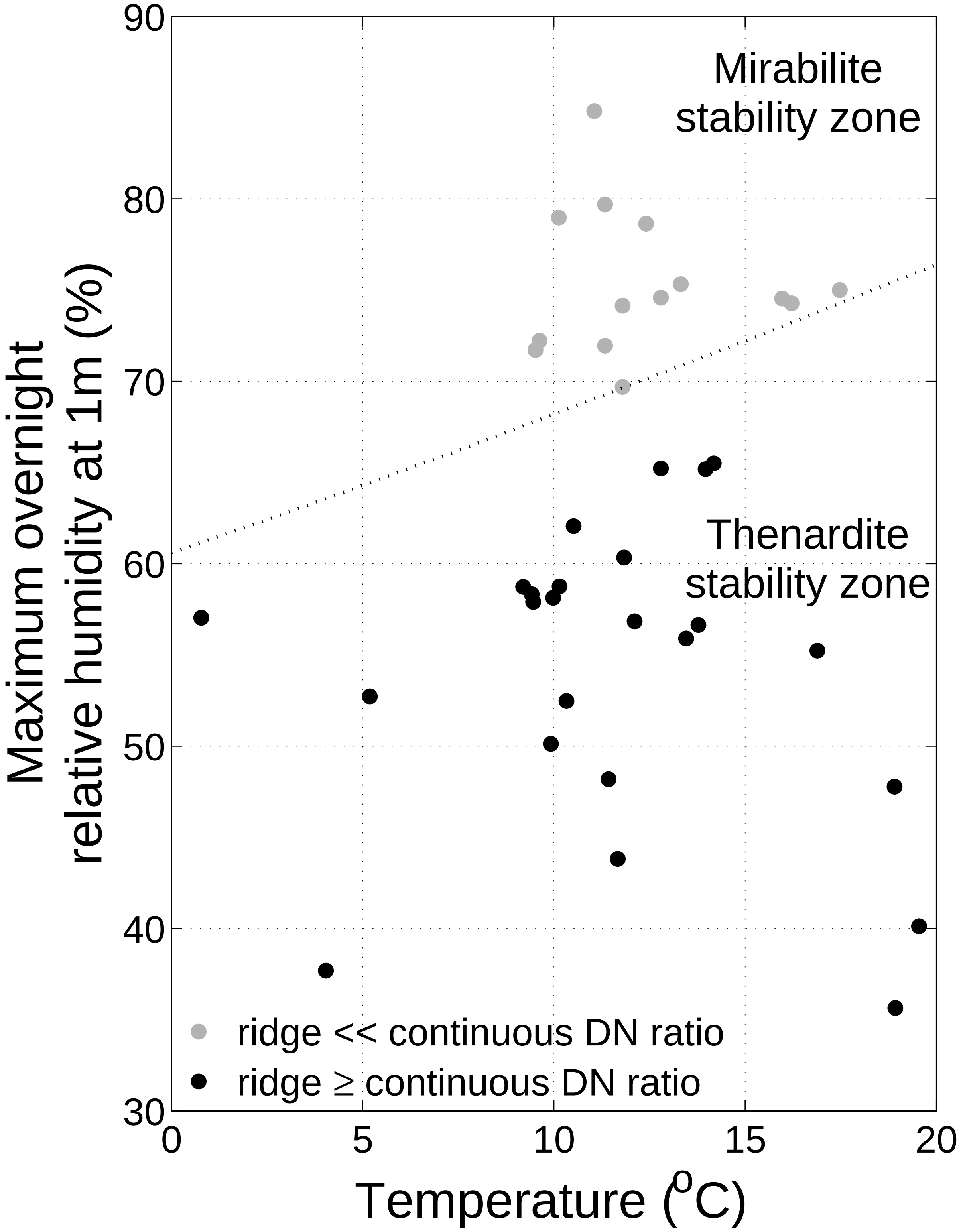

Figure 15 Maximum relative humidity (RH) value recorded each night with the corresponding temperature (T) for a 39 day infra-red camera time series. Points are separated into nights when the ridge DNR was less than the continuous DNR and nights when the ridge DNR was greater or equal to the continuous ratio

(Figure 7). The latter points independently plot within the thenardite stability zone on the sodium sulphate phase diagram and the former points well inside in the mirabilite stability zone.